UNIVERSITY OF CALIFORNIA, SANTA CRUZ

# WHAT WE CAN LEARN ABOUT THE SOURCE PROPERTIES OF TERRESTRIAL GAMMA RAY FLASHES FROM THE GROUND

by

**John Ortberg**

A dissertation submitted in partial satisfaction
of the requirements for the degree of

DOCTOR OF PHILOSOPHY

in

PHYSICS

June 2023

The Dissertation of John Ortberg is approved:

David Smith

Bruce Schumm

Steve Cummer

Peter Biehl
Vice Provost and Dean of Graduate Studies

# Contents

# List of Figures

# Abstract

What We Can Learn About the Source Properties of Terrestrial Gamma Ray Flashes From the Ground

by

John Ortberg

Terrestrial Gamma-ray Flashes (TGFs) are extremely bright, short bursts of gamma radiation associated with lightning flashes. The story of their discovery spans nearly a century and involves contributions from researchers in many different subdisciplines of physics - lightning physicists, astrophysicists, and meteorologists to name a few. This work summarizes those contributions and the evolving theories on how thunderstorms are able to generate the enormous "avalanches" of relativistic electrons responsible for the gamma rays.

This work also summarizes 3 important contributions from the Santa Cruz High Energy Atmospheric Physics group over the past 5 years:

1. Development of a new ground based detector array with µs absolute timing accuracy, large dynamic range, high resolution data during triggered events, and EMI noise sealing.
2. Quantification of the expected flux from the reverse positron beam of a TGF under the so-called "feedback model", and the detectability of such an event from various altitudes on the ground.
3. Observation of two TGFs detected from an unprecedented angle of more than 70° off the vertical axis, and Monte Carlo simulations of deviations in source parameters that could lead to the observable beam of gamma-rays reaching farther than existing theory says it should.

# 1 Introduction and Purpose

## 1.1 Definition

Terrestrial gamma ray flashes (TGFs), in short, are brief ($\approx 0.0001$ seconds), intense ($\approx 10^{17}$ gamma rays), energetic (energy distribution of $N(E) \sim e^{-\frac{E}{7.3\text{MeV}}}$) bursts of radiation associated with lightning flashes. They are rare in the context of any individual lightning flash - occurring in less than 0.1% of them - but a frequent occurrence on the planet as a whole given the global rate of several million flashes per day.

## 1.2 Motivation

Terrestrial Gamma Ray Flashes have been a subject of enthusiastic research the last few decades and to the general population it's not immediately obvious why. While the surprise and delight of finding these natural particle accelerators that produce gamma rays and positrons and neutrons at fluxes that overwhelm the capacity of even our best detectors is self evident, the decision to divert resources and attention toward a phenomena is usually subject to more scrutiny.

Any "elevator pitch" on the subject to a non-physicist will be immediately met with an optimistic question on if we can harness the energy of a TGF for our electric grid and make some money. Renewable energy sources are ideally predictable, ongoing, and easy to harness - all opposites of what you'd use to describe a TGF.

With that cleared up, I propose what I believe to be the two strongest motivations for studying TGFs:

1. **Possibility of Adverse Health Effects**

   Pallu et al. (2021) found in their simulations that regions a few 100 m long in the TGF beam produce potentially dangerous levels of radiation in humans. US Department of Commerce (2018) estimates that each commercial plane gets struck by lightning 1 to 2 times annually. With an active global fleet of around 30,000 airlines, and estimates ranging from 1 in 12,000 to 1 in 140 lightning flashes producing a TGF (Fuschino et al., 2011; Albrechtsen et al., 2019), even conservative estimates suggest there's a good chance that many people get exposed to this radiation.

   Many skyscrapers are also struck by lightning frequently - the CN Tower in Canada is

famously struck 75 times per year. The lightning protection that exists for buildings and planes is, of course, useless against gamma radiation. Since the adverse effects of radiation are generally seen years later except in extremely high, acute doses, it would not be immediately obvious to those hit by a TGF that anything was wrong.

2. **Important Role in Understanding Thunderstorms**

   Most everyone would agree it's important to be able to understand and predict thunderstorms for practical reasons, yet until recently scientists have understood embarrassingly little about how thunderstorms charge and how lightning initiates. It's no coincidence that in a period of time where we lacked the understanding to explain what can be seen (e.g. thunderstorms and lightning), we also lacked the ability to predict phenomena that can't be seen (e.g. TGFs). Any theory of how thunderstorms work is not complete if it doesn't also predict the TGFs we observe.

## 1.3 Content and Goals of Studies Performed

This work outlines 3 major contributions to advance the field of TGF research:

1. Chapter 4 details the development of a ground based detector array (THOR) with improved dynamic range, deadtime analysis, absolute time resolution, and noise reduction over previous ground based instruments.

2. Chapter 5 provides estimates of the expected brightness and detectability of the reverse positron beam of an upward TGF. These estimates are given from various altitudes on the ground, and the positrons from a feedback model TGF are used.

3. Chapter 6 reports on 2 TGFs detected on the ground from an unprecedented nadir angle of $> 70^o$. Since existing models predict a TGF would not be detectable at that angle and distance, we investigate what possible source parameters of the TGFs could produce the fluence we saw.

# 2 A brief history of TGFs

As theoretical physicist Daniel Davies once said, astrophysicists are famous for "naming things before they know what they are". As a serendipitous discovery of astrophysicists, Terrestrial Gamma-ray Flashes (TGFs) were named when little was known about their nature and even less was known about their underlying mechanism(s). While our knowledge of them has progressed, no attempt at defining a TGF can be complete without mentioning their historical context.

## 2.1 1925: C.T.R. Wilson's Hypothesis of Runaway Electrons in Thunderstorms

The field of high energy atmospheric physics can trace its origins to an early 20th century Scottish physicist by the name of C.T.R. Wilson. His early experiences as an observational meteorologist catapulted him into a career investigating the possibilities associated with the strong electric fields produced by thunderstorms. In his landmark 1925 paper, he first theorized that these fields could accelerate electrons to relativistic speeds (Wilson, 1925). Despite laying down the foundations for the field, Wilson was missing a number of important physical processes integral to the production of the high energy particles he predicted, and attempts to observe them by Schonland and Wilson (1930) inevitably came up empty. Wilson died in 1959 without ever seeing direct evidence for relativistic particles from thunderstorms, but remained confident in his theory, continuing to write papers on the topic in the years leading up to his death (Williams, 2010).

## 2.2 1960s-1990s: Double Serendipity

Ironically, the accidental discovery of TGFs actually begins with satellites that were looking in the right place. The US Military launched of a series of gamma ray detecting instruments in the VELA satellites in the 1960s for the purpose of detecting nuclear weapon testing in other countries during the cold war. A series of unexpected bursts of gamma rays were later determined to have no possible terrestrial or solar origin, leading to the 1973 paper "Observations of Gamma-Ray Bursts of Cosmic Origin" that greatly influenced the trajectory of astrophysics to this day (Klebesadel et al., 1973).

As one might expect, this 1973 paper led to the launch of new satellites, this time designed

specifically to observe these short gamma ray bursts of cosmic origin. And, also as one might expect, the satellites that were purposefully designed to study what the previous satellites had accidentally discovered in the opposite direction, these new satellites accidentally discovered something in the opposite direction of where they were purposefully designed to look. In homage to the 1973 paper, a 1994 paper titled "Discovery of Intense Gamma-Ray Flashes of Atmospheric Origin" provided the first observations of 12 TGFs collected by the Burst and Transient Source Experiment (BATSE) on NASA's Compton Gamma-Ray Observatory and launched a new field of study(Fishman et al., 1994b).

Interestingly, in between the VELA and BATSE projects, the first real observation of Wilson's relativistic electrons occurred when McCarthy and Parks (1985) reported on a long scale (several seconds) significant increase in flux of high energy X-rays while flying through a thunderstorm. Though this didn't receive the attention that the discovery of TGFs got, McCarthy and Parks did suspect this was direct observation of runaway electrons.

A key "piece of the puzzle" that had been missing from Wilson's 1925 paper but was gaining more attention at the time of the discovery of TGFs was the fact that a relativistic electron in a strong electric field would eventually create even more relativistic electrons through Møller scattering. Though Williams (2010) identifies some of Wilson's notebook entries that show his general awareness of this possibility, Gurevich et al. (1992b) formally introduced this idea of the "avalanche effect" of these relativistic electrons into the literature two years before Fishman's paper.

## 2.3 1990s-Present: Closing the Gap

The discovery of TGFs in the early 1990s proved to be a beginning rather than an end for the ideas in Wilson's 1925 paper, as evidenced by the explosion of references to Wilson's work in figure 2.2. It's no surprise that the avalanching process of relativistic electrons in air was not the only "piece of the puzzle" missing at the time of the 1994 discovery. The field that the discovery of TGFs gave rise to, High Energy Atmospheric Physics, is uniquely interdisciplinary, and the process of closing the knowledge gap with experts of its various disciplines continues to this day.

A high level overview of the knowledge gap at the time of Fishman et al. (1994b) will be given here and serve as a springboard into the next section about current state of the field and

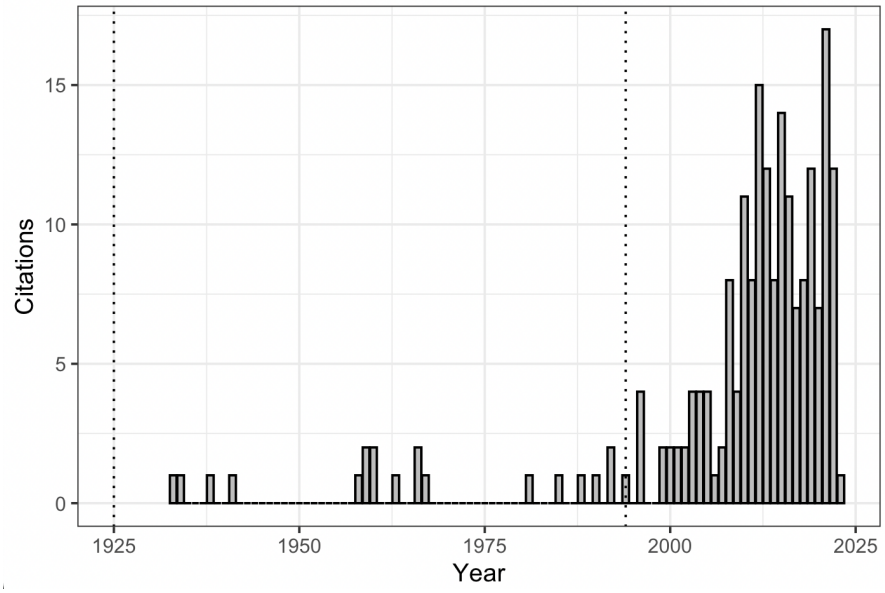


Figure 1: Number of papers citing CTR Wilson's 1925 work per year. The vertical line on the left represents the year of publication, and the line on the right represents the published discovery of TGFs.

related physics:

- **The role of high energy physics processes and streamer physics**

  Primarily looking for conditions that could lead to relativistic electrons and avalanching (RREA), early researchers pointed to electric discharges in the upper atmosphere like sprites and blue jets as the source of TGFs (Roussel-Dupré and Gurevich, 1996). Cummer et al. (2005) showed this to be incorrect by correlation between TGFs and the more familiar lightning flashes that originate in thunderclouds (with or without connection to the ground). The desire to better understand the electrical discharges associated with TGFs lead to a full investigation of the role of various high energy physics processes, streamer physics, and meteorology in producing TGFs.

- **The true brightness and intensity of TGFs**

  A likely reason that TGFs remained elusive for so long is their extreme brightness and short duration. While cosmic GRBs are much brighter at the source, TGFs are close enough to appear much brighter in Earth's orbit. Even the shortest GRBs last several milliseconds while TGFs generally last 10s of microseconds. Satellites designed to study

GRBs would therefore underestimate the total fluence in a TGF (e.g. the detectors aboard the Compton Gamma Ray Observatory in Fishman et al. (1994b) had a time resolution of $\sim 2$ µs), and to this day there are still design challenges in accurately capturing the count rate of bright and/or close TGFs.

- **The supplemental use of radio waves**

  In Fishman's paper, data from the US Lightning Detection Network was used to confirm there was lightning activity in the general time/vicinity of one TGF, and meteorological data confirmed thunderstorms in the time/vicinity of several others. Since then, the RF waves created by lightning have proved immensely valuable not just to locating individual flashes associated with TGFs but to providing insight into the behavior of the actual electrical discharges. This remains an area where our capacity to understand the data we are collecting is in its infancy.

# 3 State of the Field and Relevant Physics Processes

Still less than 30 years from the discovery of TGFs, and dependent on the collaboration of research across multiple disciplines, the field is generally considered to be in its infancy. There is still not one conclusive mechanism behind TGFs, nor is it even known if one, several, or none of the proposed mechanisms occur. One one hand, any proposed mechanism must first answer the question of "what is theoretically possible way to generate a TGF?". This is mostly done through a combination of (well-behaved) high energy particle physics and (not so well-behaved) streamer discharge physics. Then comes the question of "what does happen?", answered by a variety of observational techniques. Finally, the answer to "what is most likely to happen?" falls in the realm of meteorology, thunderstorm charge structure, and Monte Carlo simulations.

When constructing a complete picture of TGFs, meteorology is also an important place to start, any discussion of what exactly happens in high field regions of thunderstorms must first understand how the electric fields emerge to begin with and what factors contribute to the strength and structure. Thus we will first look at a broad overview of the study of thunderstorms and so-called atmospheric electricity before zooming in on the various high energy processes known or theorized to occur.

## 3.1 Thunderstorms and Atmospheric Electricity

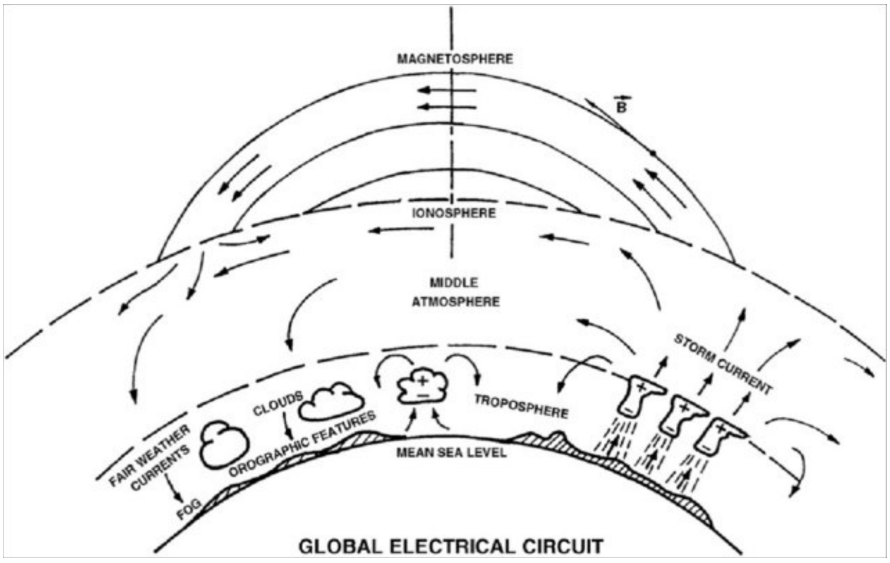


Figure 2: From Roble and Tzur (1986). This landmark paper helps to illustrate the relationship between various electrical discharge processes throughout Earth's atmosphere, and that lightning does not operate in a closed system.

Roughly speaking, updrafts in thunderstorms create and separate charged particles leading to an electric field in which a region of streamers can form. Streamers are short-lived, finger-like structures of discharge in air that have the potential to coalesce into a larger and more conductive stepped leader. These stepped leaders are generally self sufficient and will propagate towards an opposite charge center, eventually forming the lightning flash we're familiar with.

- **Thunderstorm Electrification**

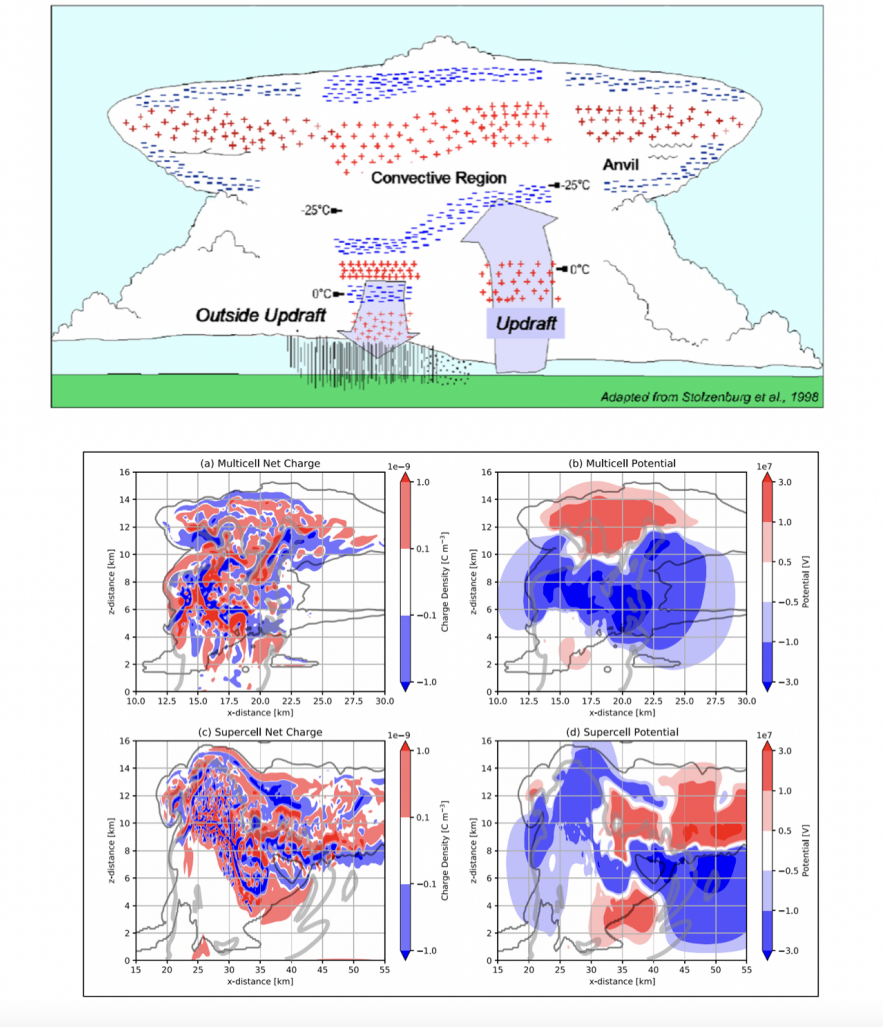


Figure 3: (top) Conceptual model based of balloon sounding data from Stolzenburg and Marshall (2008). (bottom) Simulated charge structure and electric potential of two different types of thunderstorms from Brothers et al. (2018). Note the relatively simple potential structure despite the heterogeneous charge distribution.

Despite being studied for over 200 years, there is still no complete model for thunderstorm electrification. Far from being the result of a lack of understanding, there are in fact a multitude of mechanisms that have been demonstrated to lead to charge separation in thunderstorms and the specific contribution of each remains to be determined (Saunders, 2008). The key contribution of the hydrometeors themselves (which is a fancy term for any

form of water particle in atmosphere - rain, sleet, snow, hail, etc.) in these mechanisms is that various properties such as their size, temperature, growth rate, structure, etc. lead to preferential charge structure upon collisions (Saunders, 2008; He et al., 2018). The deep convection in thunderstorms that leads to this colliding of different types of hydrometeors also helps to separate the different particles after they are charged (with lighter particles more susceptible to updraft and heavier particles more likely to fall). Large scale electric fields, including the growing thunderstorm field as well as the pre-existing fair weather field, supplement this process with various inductive charging mechanisms.

The simplest picture of the resulting charge structure of a thunderstorm is the so-called "dipole model", with a main negative charge center near the middle of the cloud and an upper positive charge center closer to the top. Despite this model's usefulness in predicting the general direction of charge transfer in lightning activity, it should come as no surprise given the complexity of charge separation mechanisms that in situ measurements pointed toward much more complicated charge structures (Stolzenburg et al., 1998; Zhang et al., 2018).

Conceptual models (Stolzenburg and Marshall, 2008) as well as more recent computer simulations (Brothers et al., 2018) have pivoted toward a much more dynamic charge distribution that still resembles the classic dipole model to first order (see figure 3). Additionally, exceptions to the dipole model have been found where thunderstorms generally exhibit a main positive charge center below an upper negative region (Stough and Carey, 2020). The cause for this relative inversion of macroscopic charge layers has been linked to conditions that reverse normal preferential charge transfer between individual hydrometeor collisions.

Direct measurements of the fields and potentials produced in thunderstorms are fairly limited in their scope - balloon measurements only travel in a vertical line and aircraft measurements inherently perturb the field with their large conducting exterior. Rakov and Uman (2003) offers a review of several electric field measurements typically in the range of $1 - 3 \times 10^5 \frac{V}{m}$, with a peak instance of $4 \times 10^5 \frac{V}{m}$ (Winn et al., 1974).

(Marshall and Stolzenburg, 2001) calculated the potential difference inside thunderstorms with a total of 15 balloon soundings, finding up to $\Delta V_{max} = 102\text{MV}$. TGFs are rare

events, and it's likely they occur in some of the more extreme fields and potentials that are unlikely to be seen in the sparse measurements that have taken place. However it's important to note that there is a fundamental limit to large scale electric fields possible in air that approaches $|\vec{E_{th}}| = 2.84\text{V m}^{-1} \cdot \frac{n(z)}{n_0}$, where $n$ is the density of air at altitude $z$ and $n_0$ the density at sea level. The total potential of a thunderstorm is naturally given an upper limit by this field strength and storm height, though it's unlikely to even get a field near the threshold to exist on a large scale (lightning is more and more likely to discharge a field the stronger and larger it gets).

- **Streamers and Lightning Initiation**

  Conventional dielectric breakdown (i.e. Townsend discharge) in air can occur when the field strength exceeds $|\vec{E_k}| \approx 3 \times 10^6 \frac{V}{m}$, more than an order of magnitude higher than fields measured in lightning producing storms as discussed above. This large discrepancy is part of the reason why lightning initiation has been such a profound mystery for years (Iudin et al., 2022).

  Streamers, on the other hand, can propagate in fields on the order of $5 \times 10^5 \frac{V}{m}$, which is much more plausible to occur in thunderstorms than conventional breakdown. In laboratory experiments, streamers are known to form at the tip of conducting electrodes when the local field allows conventional breakdown and the number of involved charges exceeds a critical value (Gallimberti et al., 2002; Cooray and Arevalo, 2017). An example of this is shown in figure 4.

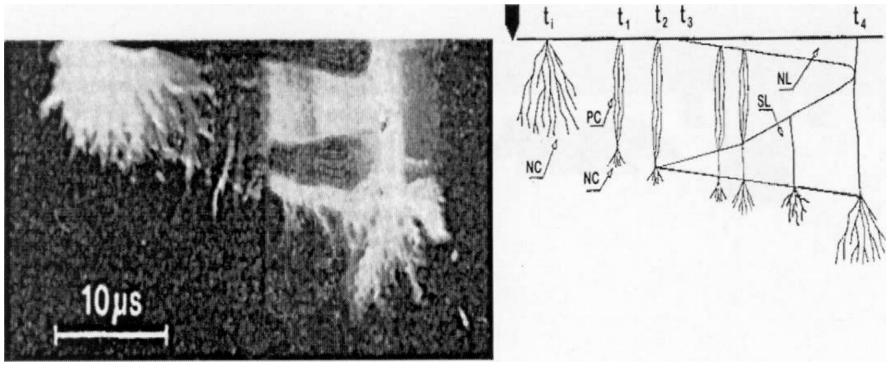


Figure 4: From Gallimberti et al. (2002). Diagram on the right is a schematic interpretation of the streak photograph on the left. Development begins with a negative corona (NC) forming on the electrode. Streamers from the negative corona coalesce to form a space leader (SL), which eventually connects with the negative leader (NL) growing from the electrode.

> In thunderstorms, a series of very small corona discharges from hydrometer collisions increases in size by about two orders of magnitude to eventually create a network of streamers (Iudin et al., 2022). This network of streamers can coalesce into a large, hot, conductive channel called a leader, which will then travel in a series of steps toward an opposing charge structure as part of the lightning discharge process (Cooray and Arevalo, 2017). Importantly, both leaders and streamers enhance the $\vec{E}$ field in the air around them in order to achieve self-sustaining propagation provided sufficient conditions (which can include things like background field, supply of free charges, etc.).

The nature of these electric fields and electrical discharges in air the occur in thunderstorms are important to understand as we build a framework for the high energy processes that are thought to contribute to TGFs. Electric field strength, structure, and the nature of streamer/leader discharge help determine the mechanism(s) behind TGF production.

## 3.2 TGF Building Blocks

- **Runaway Electrons**

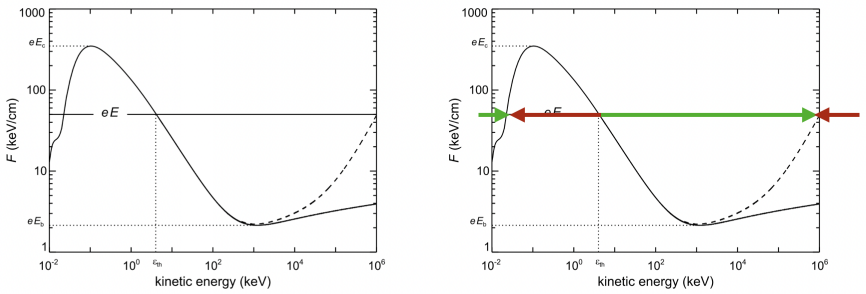


Figure 5: From Dwyer and Smith (2005). Solid curve is the frictional force of air on an electron due to inelastic collisions. The dashed line is the sum of that force plus the effect of radiative losses (bremsstrahlung). The horizontal line considers the effect of an electric field of strength E on the electron. The arrows on the right panel show how the combined effects either speed up (green) or slow down (red) an electron to reach equilibrium. The equilibrium on the right would be considered the "runaway" regime.

The concept, first introduced by Wilson (1925), is simple: while normally an electron experiences a stronger frictional force the faster it goes, that frictional force will actually start *decreasing* with speed past a certain point ($\sim$ 10 eV) towards an eventual minimum near 1.5 MeV.

Here it's important to note that the term "friction" in this field is often used to mean the "stopping power" that's actually caused by molecular excitation, ionization, and bremsstrahlung as the electron moves through atmosphere. This stopping power, described by the Bethe formula, falls quadratically with electron speed until it reaches a valley around 1.5 MeV, where radiative losses (bremsstrahlung) and higher order effects of the Bethe formula once again begin to increase the stopping power.

In simpler terms: any electron already traveling fast enough to have its frictional force be below that of the $\vec{E}$ field force will continue traveling at relativistic speeds and accelerate to equilibrium. Figure 5 shows the non-relativisitic and relativistic equilibria that emerge in fields above $\vec{E_{th}}$.

It's important to note that $\vec{E_{th}}$, whose magnitude is $2.84 \times 10^5 \frac{V}{m}$ at sea level, is about 25% stronger than predicted by Wilson (1925) since electrons are not only slowed down by

air molecules but also have their velocity diverted away from electric field lines (Dwyer, 2003). $\vec{E_{th}}$ decreases with decreasing air density; the "sea level equivalent" of an electric field at altitude is obtained scaling for the density at that altitude relative to sea level, i.e. $\vec{E_{eq}} = \vec{E}\frac{n}{n_0}$ (Dwyer, 2012).

There's no doubt that electrons in the runaway regime are the source of gamma-rays in TGFs (via bremsstrahlung radiation), but even if a field above $\vec{E_{th}}$ exists on a large scale only relativistic electrons will be affected. A source on the order of $10^{17}$ relativistic electrons is still required.

- **Relativistic Runaway Electron Avalanches (RREA)**

  Relativistic electrons will free electrons in air molecules via Møller Scattering. If both electrons end up above $\epsilon_{th}$, they will both continue to run away. Gurevich et al. (1992a) identified and described this relationship with the simple equation

$$N(s) = N_o \exp(\frac{s}{\lambda}),$$

  where $N$ is the number of electrons above $\epsilon_{th}$, $N_0$ is the number of initial electrons above $\epsilon_{th}$ (often called the "seed electrons"), $s$ is the distance in a uniform electric field, and $\lambda$ is the characteristic "avalanche" length.

  An important feature of this RREA process is that while the avalanche length $\lambda$ depends on the strength of the electric field, the energy spectrum $f(\epsilon) \sim \exp(\frac{-\epsilon}{7.3\text{MeV}})$ is nearly independent of it (Roussel-Dupré and Gurevich, 1996; Babich et al., 1998; Dwyer, 2003).

  While it takes only 1 relativistic seed electron ($N_0 = 1$) to achieve this avalanche multiplication, reaching a common brightness of $10^{17}$ relativistic electrons in a TGF would require the "avalanche region" to be $s_{max} = \ln 10^{17} \cdot \lambda \approx 40\lambda$. The $\vec{E}$ field required to make 40 avalanche lengths would have to be too strong, too large, or both to be possible in a thunderstorm. Carlson et al. (2009) estimates that thunderstorm fields could multiply each seed electron by a factor of at most $10^5$ ($\gamma \leq 11$). There must exist a separate large source of seed electrons.

- **Feedback**

Dwyer (2003) identified two ways in which a relativistic runaway electron avalanche could potentially create its own seed electrons (illustrated in Figure 3.2):

1. Backscattered gamma-rays that travel back toward the start of the avalanche region can create new energetic electrons via Compton scattering or photoelectric absorption.
2. Positrons, created by pair production from bremsstrahlung gammas, will naturally accelerate toward the start of the avalanche region. There they can create seed electrons directly through Bhabha scattering or indirectly by making a high energy gamma-ray through annihilation or bremsstrahlung.

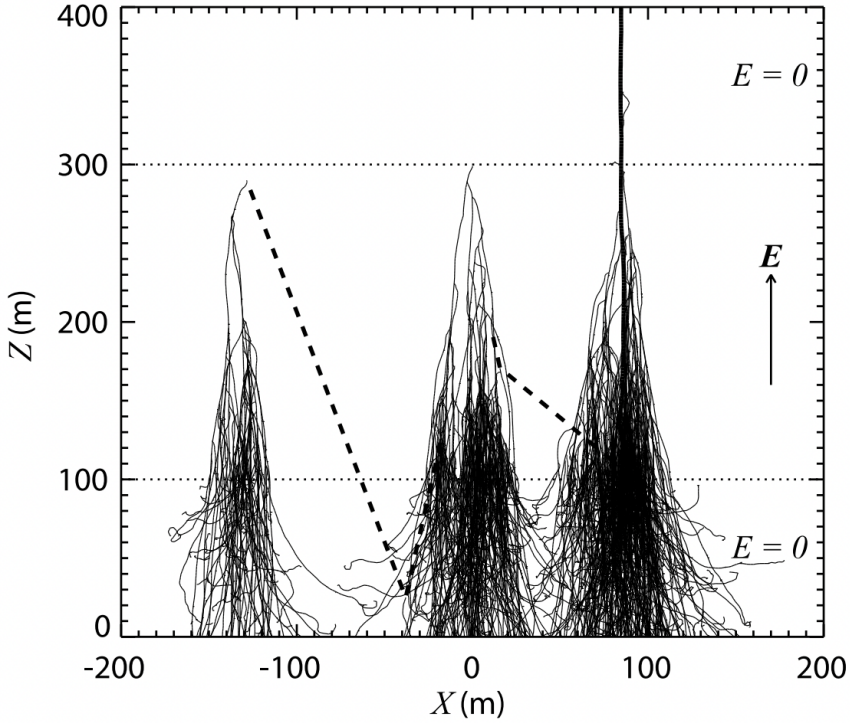


Figure 6: From Dwyer (2003). Thin black lines represent relativistic electrons in the RREA process. Dotted lines are gamma-rays that propagated toward the start of the avalanche region and created a new seed particle, and the thick black line is a positron that did the same thing but was accelerated upward in the strong $\vec{E}$ field.

Dwyer introduces a feedback factor $\gamma$ to quantify the expected value of new seed electrons

created per seed electron. When $\gamma$ is greater than 1, the number of relativistic electrons will increase exponentially until enough charge is moved to reduce the field below $\vec{E_{th}}$. The simple model used for RREA now becomes

$$N(s,t) = \gamma^{\frac{t}{\tau}} \exp\left(\frac{s}{\lambda}\right)$$

where $\tau$ is the characteristic time for one seed electron and all its secondaries to finish propagating through the avalanche region.

In this mechanism, the peak flux of any gamma-ray activity would depend not on the number of seed electrons but rather on the feedback factor and characteristic avalanche time/length. It's also important to note this model predicts a smooth time profile of gamma-ray flux and that feedback growth ($\gamma > 1$) only occurs for some minimum combination of length, volume, and strength of RREA field (Dwyer, 2012).

Feedback has primarily been studied in the context of uniform $\vec{E}$ fields, however more recently Stadnichuk et al. (2021) examined the possibility of feedback between multiple field regions with various orientations in close proximity. Depending on the geometry, the number of gamma-rays beamed in a direction to continue the feedback process would be much greater than traditional feedback where only backscattered gammas (and positrons, as mentioned above) can create new seed particles.

- **Cold Runaway**

  At fields stronger than $2.6 \times 10^7 \frac{V}{m}$, the electric force is stronger than dynamic friction for all free electrons in air, and all free electrons will therefore experience runaway to relativistic energies.

  Such fields don't exist in a large scale, but are thought to be possible at the tips of highly conductive lightning leader channels (Moss et al., 2006). This would potentially create a sizeable population of highly energetic seed electrons ($n_e \approx 10^{12}$), which would then require a much smaller RREA field ($L \approx 5\lambda$) to achieve normal TGF brightness through avalanche multiplication (Carlson et al., 2009,0).

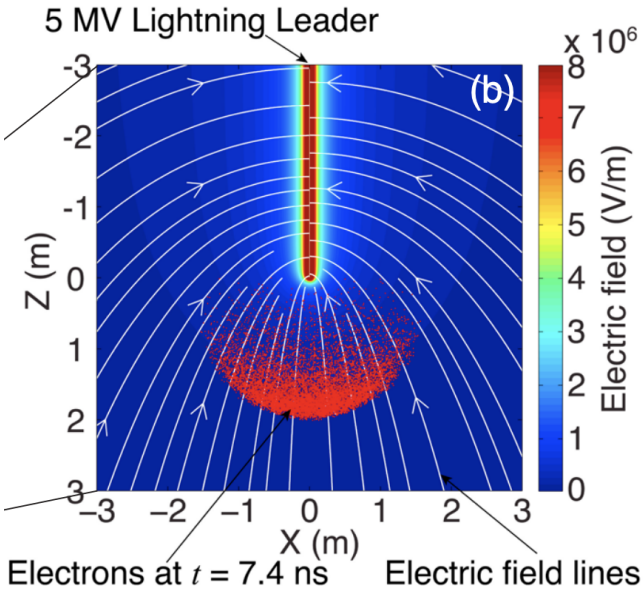


Figure 7: From Xu et al. (2014). Free electrons (red dots) undergo "cold runaway" in the enhanced field surround a lightning leader.

Since RREA electrons travel at roughly the speed of light, the time scale of a TGF seeded purely by cold runaway should match the time scale of the high field region in the leader supplying the current pulse. The duration of stepped leaders is generally around a few µs, $10^2$ µs for initial return strokes, and a few µs for lightning processes that occur after charge center connection (e.g. so-called "dart leaders" and "M-components" as well as subsequent return strokes) (Carlson et al., 2009; Rakov and Uman, 2003). However, any electric field strong enough to support cold runaway would likely only last for a part of those processes if it emerges at all.

In the criteria for whether or not cold runaway produces a TGF, only the number of avalanches in the RREA region matters, as opposed to feedback where the geometry of the region determines whether or not $\gamma > 1$. Therefore it is possible, though not necessarily true, for the angular distribution of a "cold runaway TGF" to differ from that of a "feedback TGF".

- **Intensity and Duration**

As one might expect, the above mechanisms don't necessarily require that gamma rays

are produced in extremely bright, short bursts. Without covering all of the theoretical possibilities, the observations of gamma ray events so far can be categorized in three ways based on intensity, spectrum, and duration:

1. Modification of Spectrum (MOS) occurs when any thunderstorm electric field is not strong enough to support relativistic runaway, but is strong enough to noticeably shift the background cosmic ray spectrum to slightly higher energies (Chilingarian et al., 2013).
2. Glows occur when the background electric field does support RREA, but the brightness is within a factor of 1-100 of that of background radiation, and the timescale is generally seconds to minutes.
3. TGFs are the bright, submillisecond flashes of gamma radiation, and there appears to be a lack of intermediate events that would lie in between the brightness/timescale spectrum of glows and TGFs.

- **TGFs as Earth's Particle Accelerator**

  At 10s of MeV, the high energy electrons in TGFs are not limited to bremsstrahlung radiation. Wilson (1925) predicted the occurrence of nuclear reactions in the high field regions of thunderstorms, and although the mechanism he suggested turned out to be impossible, other mechanisms were found to plausibly generate free neutrons in TGFs (Babich et al., 2007).

  **Neutrons** are created by photons of 10 MeV or more knocking them loose from nitrogen atoms ($^{14}N + \gamma \rightarrow^{13} N + n$). Free neutrons in the atmosphere will, on the time scale of $10^{-1} - 10^{0}$ seconds, thermalize with ambient air and attach to a hydrogen atom (thereby creating deuterium). This neutron capture releases a 2.23 MeV gamma ray, and as such a long signal of gammas $\leq$ 2.23 MeV is evidence of neutrons from a TGF that can be detected without the concern of dead time or detector paralysis that normally plagues TGF detection (Wada et al., 2022).

  **Positrons** can come from that same mechanism on the same longer timescale, where the newly created $^{13}N$ nucleus undergoes beta decay. Any gamma above 1.1 MeV can interact with a nucleus to create a positron/electron pair, which creates a significant population

of positrons on the same timescale as the TGF itself. Some of these positrons would be integral to the feedback process as discussed in section 3.2, but a population of these positrons would exist regardless of whether or not feedback was the primary driver of the TGF.

## 3.3 TGF Detection

In addition to being completely accidental, early TGF detection was quite primitive. The challenge of effective TGF detection is two-fold: (1) managing to get an accurate gamma-ray count given their high intensity and short duration, and (2) being in the right place at the right time to capture what is, relative to normal lightning flashes, a rare phenomenon.

- **Gamma-ray Detection**

  Gamma rays must be detected through indirect processes such as scintillation, ionization chambers, cherenkov radiation (generally through water tanks), or solid state detectors. In scintillation, a gamma ray hits a material that can absorb its energy and re-emit it as visible light. This re-emitted light then enters a photomultiplier tube (PMT), where it triggers a cascade of electrons through a series of dynodes to eventually create a current pulse. The other three methods create a similar current pulse but through other means. This current pulse is usually digitized and stored on a computer hard drive, as there's not enough space/processing power to continuously save the digitized current.

  Not only does the light emitted by the scintillating material have a characteristic time profile (which varies by material), but so does the PMT's electron cascade on its own. The resulting current pulse is thus a convolution of the scintillation light and the PMT cascade; both pulses have a fast rise and slow decay.

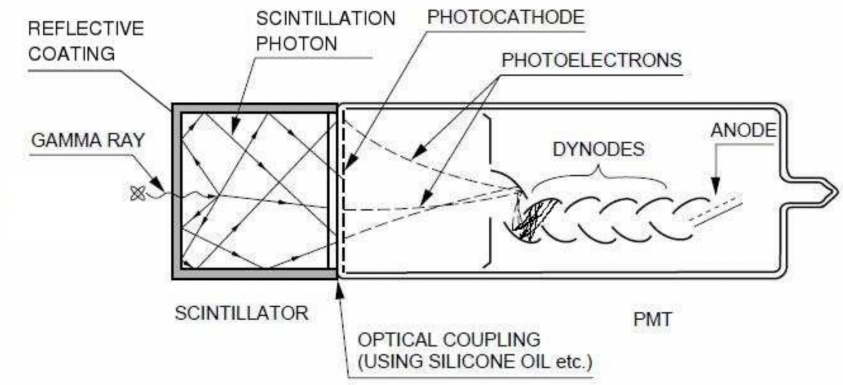


Figure 8: From Régis (2011).

If a second photon deposits energy in the scintillator before the pulse from the previous photon has returned to baseline, the two pulses will get superimposed. Data must generally be collected at a rate and volume the precludes saving detailed pulse shapes, so decomposition of these "piled up" pulses is often not possible.

This can result in several superimposed pulses being recorded as one large pulse, underestimating the gamma ray flux and overestimating the average energy. In addition to this effect being partially responsible for the underestimation of TGF brightness in Fishman et al. (1994b), it also famously lead to a false discovery of 100 MeV photons that was later retracted in Marisaldi et al. (2019).

- **Detecting From Above**

  Satellites are without question the most efficient way to detect the highest number of TGFs. At low earth orbit they have a flat detection efficiency from about 0-300 km off nadir with a slow drop in efficiency going out to 800 km (Briggs et al., 2013).

  BATSE (Fishman et al., 1994b), RHESSI (Smith et al., 2005), AGILE (Marisaldi et al., 2010), Fermi (Briggs et al., 2013), and ASIM (Østgaard et al., 2015) have combined to record tens of thousands of TGFs between them. The downside of satellite detection is that by the time the gamma-rays arrive they've been largely compton scattered, decreased in density, and there's no chance to observe photonuclear reactions or positrons.

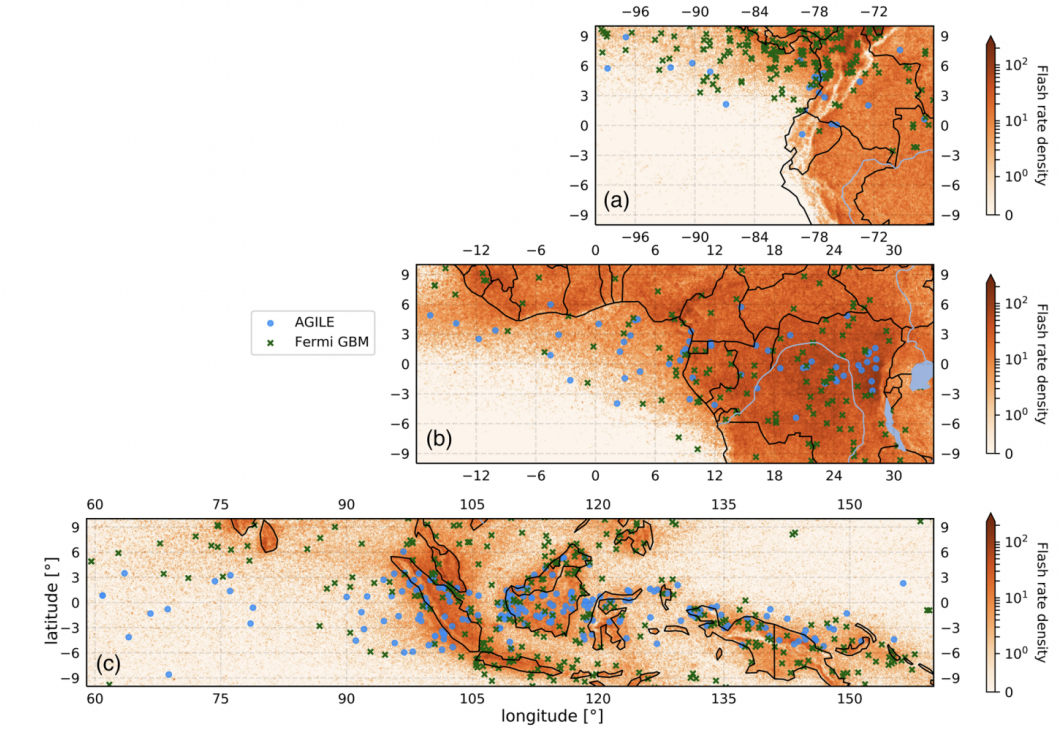


Figure 9: Plot of geographic distribution of TGFs as recorded by satellites Fermi and AGILE from Lindanger et al. (2020). Although the have different oribital inclinations, a general trend of the TGF:lightning ratio being higher in tropical coastal regions over oceanic or landlocked regions has been observed. Fabró et al. (2019) hypothesizes that the larger structure of coastal storms makes them more likely to produce energetic flashes associated with TGFs.

- **Detecting From Below**

  Detections on the ground will are much closer to the source and allow for direct control over where to look for TGFs versus satellites. Greater care must be taken to mitigate effects of deadtime due to the extreme brightness, and TGFs more than a few kilometers away won't be seen. As a result, far fewer (less than 100) TGFs have been detected from the ground, but in general far more is known about each of those TGFs.

  While the brightness of TGFs poses a challenge, the increased proximity with ground detections has allowed for the discovery of fainter events not seen from space: gamma-ray glows (chu, 2000; Torii et al., 2011). Gamma-ray glows are significantly longer lasting and lower luminosity bursts of gamma-rays from high field regions in thunderstorms, generally

lasting seconds or minutes and producing fluxes comparable to or within an order of magnitude of the background count rate at the ground (Tsuchiya et al., 2011). It is thought that same glow events may involve only RREA multiplication, while brighter events may have significant feedback with a $\gamma$ factor around 1.

Observations of gamma ray glows being terminated by a lightning strike that also produces a TGF reinforces the idea that a lightning leader entering a strong RREA field is the driving cause behind TGFs (Smith et al., 2018; Wada et al., 2019a). Background cosmic ray flux is generally sufficient at providing seed electrons for these gamma-ray glows, and even fields below the RREA threshold are capable of slightly modifying the background spectrum (Chilingarian et al., 2013). Some properties of the electric field in the thundercloud can be deduced with precise measurements of the modification of that background spectrum over time (Hariharan et al., 2019).

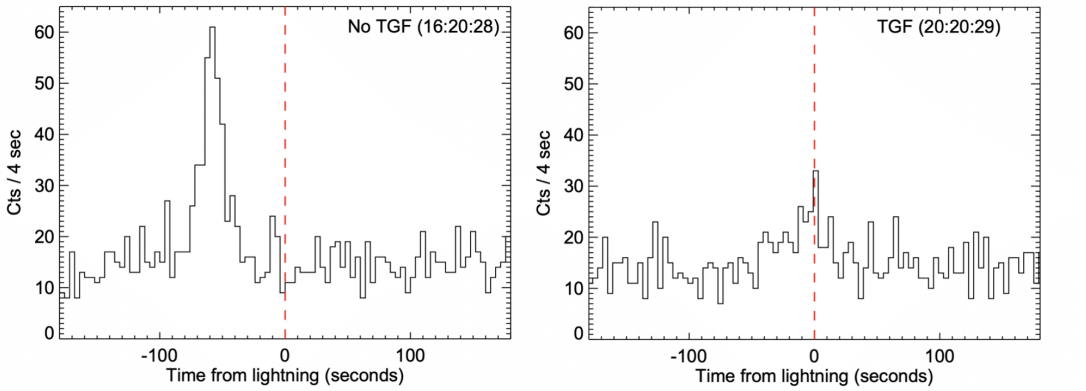


Figure 10: From Smith et al. (2018). In two nearly identical lightning strikes to a wind turbine on the west coast of Japan, a strong glow terminates before the flash resulting in no TGF, while a weak glow terminates simultaneously with the TGF flash. This suggests that the lightning leader entering the RREA field region producing the glow is what causes the TGF.

- **Detecting From Within**

  Detectors above aircraft have the obvious advantage of being able to target specific storms and the obvious disadvantage of being extremely expensive to operate. The "detectable radius" will be similar to that of ground deployments.

McCarthy and Parks (1985) detected what was likely a gamma ray glow many years before TGFs were discovered, and correctly noted that the glow's abrupt termination, coincident with a lightning flash, must've been temporal rather than a result of the plane exiting the glow region.

While ground detections are, as previously mentioned, much closer to the source than satellite detections, aircraft will have access to particles beamed upward that ground deployments will miss. While this would normally mean seeing the main upward beams of +IC TGFs, Bowers et al. (2017) observed a the downward beam of a +IC TGF from below - the significance of this discovery is that it would imply a large population of positrons to create such a large downward directed flux. The existence of such a large population of positrons favors the feedback mechanism.

## 3.4 The Role of Radio Waves

In Fishman et al. (1994b), the only positive link between TGFs and lightning activity was made through a general correlation of the satellite position with regions of high average lightning flash rate, and a few TGFs that were confirmed to have been recorded over regions of active thunderstorms. Because of the lack of precision of association between TGFs and lightning activity, the (incorrect) notion that TGFs were associated with electrical discharges in the upper atmosphere (sprites) persisted for some time. This idea was attractive in part because it meant the gamma rays would have less atmosphere to travel through to reach satellite level and therefore required a lower intrinsic brightness of TGFs. Even when some of the first recorded TGFs were associated in time with lightning flashes (Inan et al., 1996), it was still consistent with the idea that sprites, which can be nearly simultaneous with individual lightning flashes, were the source of gamma rays.

That paradigm began to shift when a rocket triggered lightning event in Florida generated a downward TGF (Dwyer, 2004). That TGF had to have originated *in* the thundercloud rather than above it, and although that didn't preclude the possibility that high altitude sprites could generate TGFs, it shifted attention toward the idea that TGFs occur deeper (lower) in the atmosphere than previously thought. This investigation would end up relying heavily on localizing the lightning activity associated with TGFs through the use of radio data.

VLF (very low frequency) and LF (low frequency) categories will be used to refer to frequencies in the kHz and 10s of kHz range, respectively. VHF (very high frequency) will generally refer to the MHz range.

**LF Radio Emissions**

Lightning produces radiation in a broad range of the electromagnetic spectrum, far beyond the visible light it's famous for. The radio spectrum of the pulses created by lightning are broadly known as "sferics", short for "radio atmospheric signal". Throughout the late 20th century, techniques were developed to use these sferics to locate the source of lightning activity in space and time.

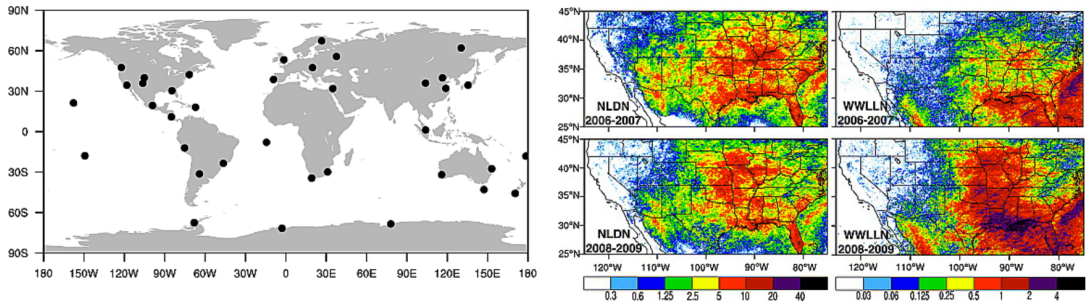


Figure 11: Abarca et al. (2010) reports the locations of the World Wide Lightning Location Network (WWLLN) sensors at the time (left) as well as a comparison of flash rates reported by WWLLN vs. the US National Lightning Detection Network (NLDN). Although LF/VLF lightning radiation can be detected from large distances, the efficiency of these lightning detection networks is constantly being improved.

Longer lightning channels in CG and IC flashes create powerful LF/VLF radiation with minimal attenuation that can be used for localization from 100s or even 1000s of km away. So-called lightning location networks such as WWLLN (see figure 11) use an array of spatially separated broadband antennae to offer localiziation over broad geographic areas.

Shortly after a catalogue of TGFs from the satellite RHESSI was published (Smith et al., 2005), Cummer et al. (2005) and Stanley et al. (2006b) found sferics of the associated lightning flashes and constrained the source altitudes to near thundercloud levels. This is well (10s of km) below the altitude of sprites, where TGFs were thought to originate at the time. This discovery had implications not only for the mechanism of TGF production, but also for their intrinsic

birghtness. TGFs would have to be much brighter than previously thought in order to produce the fluxes observed at satellite level from deeper in the atmosphere.

Cummer et al. (2015) analyzed the LF signals of 3 lightning flashes associated with TGFs detected by Fermi. They noted the TGFs were all produced around the mid portion of these several km long upward stepped leaders, and that these leaders propagated an entire order of magnitude faster than the observed average leader speed. The 3 TGFs occured when the leader tip was between 8-11 km altitude.

**VHF Radio Emissions**

Charge acceleration on shorter scales - such as that which occurs in streamers and leader steps (at the moment of stepping) - produces VHF radiation that can't be seen from as far but allows for much greater spatial and temporal resolution. Systems of VHF antennas - known as lightning mapping arrays (LMAs) - allow for the 3-D reconstruction of not only the structure of a lightning flash but the surrounding charge structure as well (Rison et al., 1999).

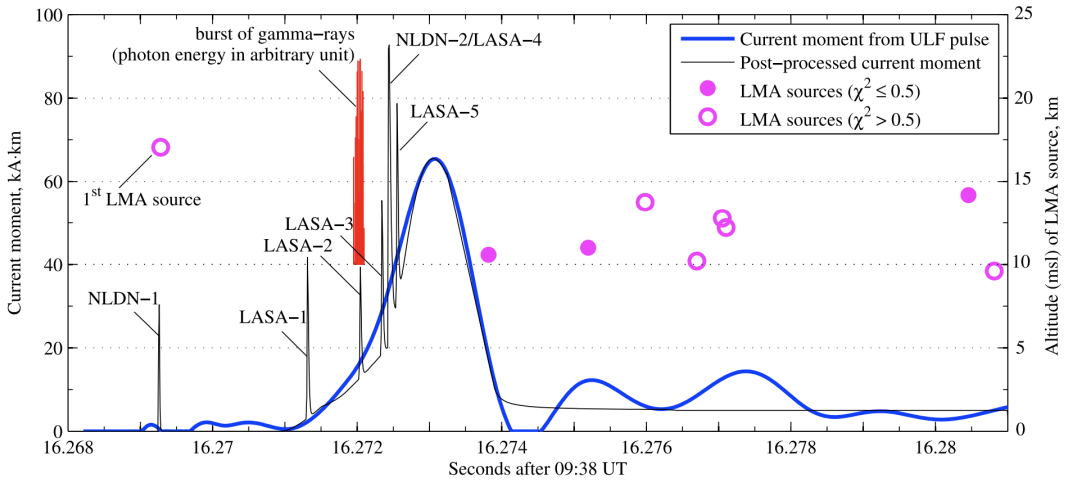


Figure 12: From Lu et al. (2010). With synchronized data between RHESSI and the North Alabama LMA, the production of the gamma-rays of this particular TGF/IC flash are shown in context of the evolution of the lightning flash. The gamma-rays appear to be produced in the early stages of development of the upward leader.

While the ionosphere and ground act as an efficient waveguide for LF waves, the same is not true for VHF waves and as a result VHF energy attenuates much faster. But while far fewer

TGFs occur in range of VHF arrays vs. LF arrays, these VHF arrays allow for far greater detail when they do detect TGF associated flashes. Lu et al. (2010) found that one of the flashes recorded at the North Alabama LMA was concurrent with a TGF detection from RHESSI while overhead. With the enhanced spatial and temporal resolution of the LMA they were able to identify the altitude and charge moment of the upward leader of the flash when the TGF occurred.

**Waveform Analysis**

These sferics are classical in nature and can be described in terms of the source currents and charges that make them using Jefimenko's Equations:

$$\mathbf{E}(\mathbf{r},t) = \frac{1}{4\pi\epsilon_0}\int\left[\hat{\mathbf{R}}\left(\frac{\rho(\mathbf{r}',t')}{R^2}+\frac{1}{cR}\frac{\partial\rho(\mathbf{r}',t')}{\partial t}\right)-\frac{1}{c^2R}\frac{\partial\mathbf{J}(\mathbf{r}',t')}{\partial t}\right]d^3r'$$

$$\mathbf{B}(\mathbf{r},t) = \frac{1}{4\pi}\int\left(\frac{\mathbf{J}(\mathbf{r}',t')}{R^2}+\frac{1}{cR}\frac{\partial\mathbf{J}(\mathbf{r}',t')}{\partial t}\right)\times\mathbf{R}\;d^3r'$$

where $\mathbf{r}'$ represents the position of the charges and currents, $t'$ represents the retarded time, and $\mathbf{R} = \mathbf{r} - \mathbf{r}'$. It is, of course, much more straightforward to calculate the $\mathbf{E}$ and $\mathbf{B}$ fields for a given set of currents then to reconstruct the source currents given a measurement of the fields. Much work was done in the 1970s and 1980s to identify the characteristics of the waveforms of intracloud (IC) vs. cloud-to-ground (CG) flashes (Krider and Radda, 1975; Uman et al., 1976; Lin et al., 1979), accounting for effects like ground attenuation, ionospheric reflection, etc, but a foolproof metric for distinguishing the two remains elusive. Even in modern lightning detection networks, CG and IC flashes are sometimes misclassified in automated waveform analysis. Many of these networks are now turning to machine learning based off of manual classification (Zhu et al., 2021).

TGFs themselves have characteristic currents that in theory produce characteristic waveforms. Dwyer and Cummer (2013) calculate a comphrensive model of what the waveform of such currents would look like to distant lightning detection radio antennae, taking care to model the current profiles of all proposed TGF mechanisms. But even if those predictions are accurate the lightning activity concurrent with TGFs will create unpredictable signals in the radio spectrum that may obfuscate the TGF current signature beyond recognition.

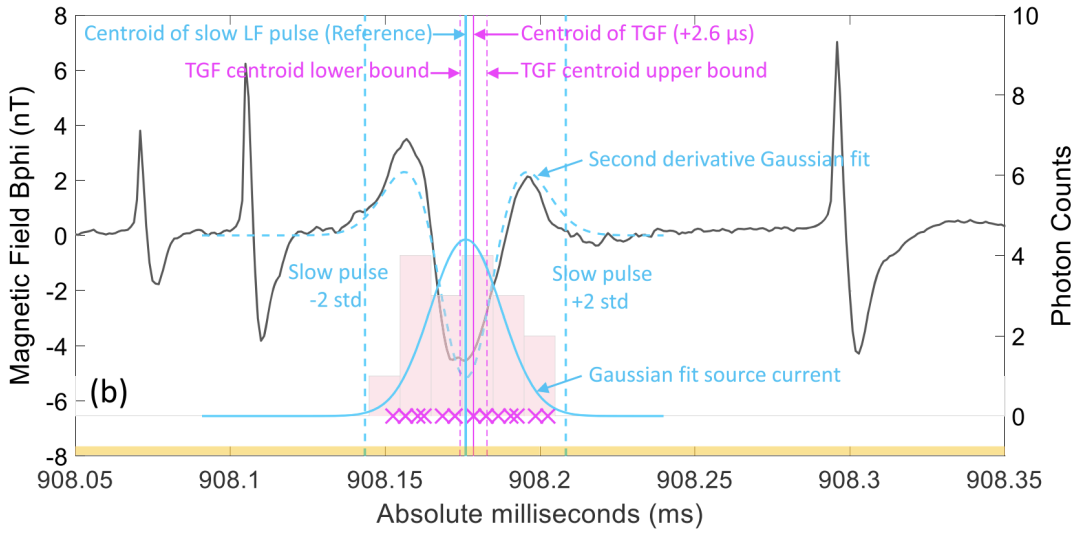


Figure 13: Pu et al. (2019) reports the observation of an LF waveform that is both simultaneous with the prodcution of a TGF and consistent with what the currents of a TGF are predicted to produce.

Nonetheless multiple TGF waveforms have been associated with TGFs, the most notable of which is the Energetic In-Cloud Pulse (EIP) described by Lyu et al. (2015) which were found to always be associated with a TGF when they occured (Lyu et al., 2016), though not all TGFs are associated with EIPs. Importantly EIPs were determined to *not* be caused by the source currents of TGFs, partially due to the lack of correlation between the brightness of a TGF and its associated EIP. Pu et al. (2019) found a radio signature (called a "slow pulse", shown in 13) that appeared to be simultaneous with TGF production and fit with the radio waveform expected from a feedback mechanism TGF. Research in this field is still in its infancy; an assortment of sferics related to TGFs are characterized in table 1.

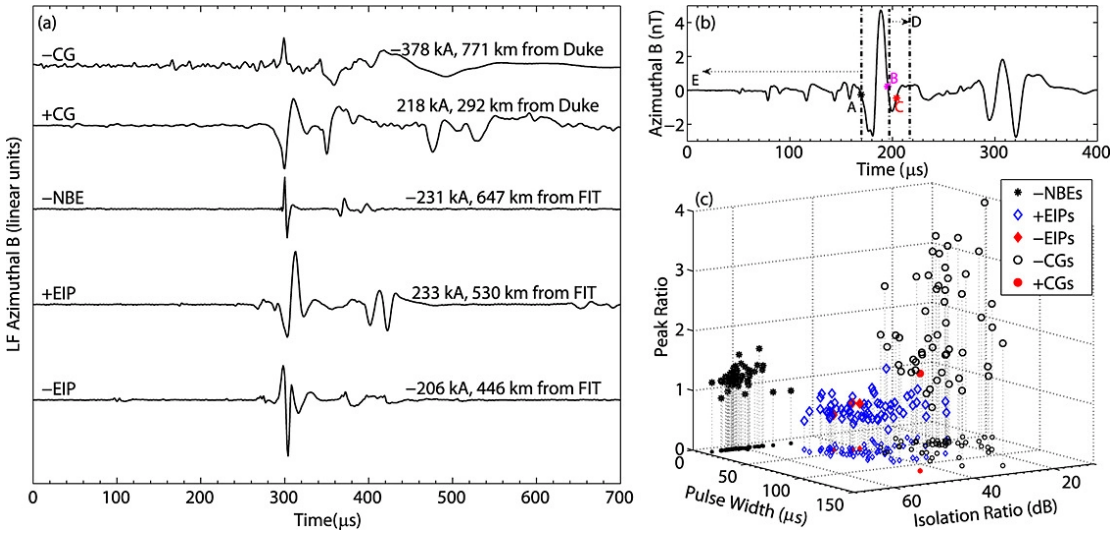


Figure 14: Lyu et al. (2015) shows the quantitative parameter space of several different sferics.

### Optical Emissions

Although lighting's emissions in the radio spectrum are by far the most easiest to detect from anywhere on Earth as they travel through the previously mentioned natural wave guide, activity at other frequencies can be useful in unique ways. In the optical range, for example, Janda et al. (2012) demonstrated via labratory experiments that streamer activity produces a strong 337 nm line while hot, conductive channels like leaders do the same at 777 nm. ASIM has installed optical sensors at these two wavelengths to identify lightning activity in sync with its gamma-ray detectors on board (Østgaard et al., 2019).

| Name | Characteristics | Approximate Pulse Width | Key Papers |
|---|---|---|---|
| Narrow Bipolar Events (NBEs) | - Occurs during lightning initiation<br>- Associated with positive and (more recently) negative fast breakdown<br>- Sometimes *preceeded* by a TGF | $10\mu s$ | - Zhang et al. (2021)<br>- Rison et al. (2016) |
| Energetic In-cloud Pulses (EIPs) | - +EIPs have found to all been linked to TGFs, though not all TGFs have EIPs.<br>- -EIPs hypothesized to have downward TGFs not seen by satellite<br>- Not due to currents inside the TGF | $20-70\mu s$ | - Lyu et al. (2015)<br>- Lyu and Cummer (2018) |
| Mountaintop Energetic Pulses (MEPs) | - Large bipolar pulses seen over mountainous regions in western US<br>- Thought to be associated with terrain initiated upward leaders<br>- Hypothesized to be associated with downward TGFs (not visible by satellite) | $20-70\mu s$ | - Lyu et al. (2021) |
| Large Bipolar Events (LBEs) | - Large bipolar pulses seen on the west coast of Japan in winter<br>- Found to be a subset of Compact Return Strokes<br>- Similar characteristics to MEPs<br>- Some associated with TGFs | $20-50\mu s$ | - Wu et al. (2014)<br>- Wu et al. (2021b) |
| Slow Pulse | - Long, smooth LF pulse on the timescale of and coinicdent with gamma-ray production in TGFs.<br>- Believed to be created from the current of the electron avalanches inside the TGF itself. | $80\mu s$ | - Pu et al. (2019) |

Table 1: List of selected sferics relevant to TGFs

# 4 Santa Cruz High Energy Atmospheric Physics (HEAP) Group

Our group's primary contribution to the field comes in the development and deployment of gamma-ray detectors to areas of high interest for TGF activity **on the ground**. The benefits and challenges of ground detections in the context of the state of the field as a whole are discussed in section 3.3. Before the development of the detector array THOR (Terrestrial High-energy Observations of Radiation), our group has been using a number of instruments that were designed in the early/mid 2010s for ground or aircraft based gamma-ray detections.

## 4.1 Previous Instruments

There are two features common in most of these instruments.

The first is the concurrent use of plastic and NaI detectors. Plastic provides great time resolution (imperative for bright TGFs) but has poor energy resolution. NaI provides good energy resolution but has poor time resolution.

The second is the use of different sized detectors to achieve a high "**dynamic range**". The dynamic range we're interested in with regards to TGFs is the ratio of the highest to lowest gamma-ray flux ($\frac{\text{counts}}{\text{cm}^2\,\text{s}}$). While the electronics of any detector system have a maximum count rate before they experience deadtime and/or paralysis, the actual count rate deposited in any scintillator $R$ is a product of the natural flux $\Phi$ and its effective area $A_{\text{eff}}$:

$$\Phi = \frac{R}{A_{\text{eff}}}.$$

Therefore even if $R$ is constrained to a small range, we can have a larger dynamic range for $\Phi$ by having multiple detectors with different $A_{\text{eff}}$ values.

**ADELE**

The Airborne Detector for Energetic Lightning Emissions (ADELE) was a large (and heavy!) array of plastic and NaI scintillators that could achieve a fast count rate at the expense of energy resolution, using only 4 energy channels. It was designed for use in aircraft and captured what appeared to be the reverse positron beam of a TGF while on board the NOAA Hurricane Hunter's aircraft in 2015 (Bowers et al., 2018).

**GODOT**

The Gamma ray Observations During Overhead Thunderstorms (GODOT) was developed shortly after ADELE and featured improved energy resolution (4028 channels) at the cost of a slightly lower maximum count rate. It also had additional tools for monitoring electrical noise/interference. GODOT was deployed to Uchinada on the west coast of Japan, a coastal region famous for its low winter thunderstorms (due to cold air from the Asian mainland that blows over the relatively warm Sea of Japan). It was here that we saw a TGF that was notable for (1) producing neutrons observed by GODOT (Bowers et al., 2017) and (2) terminating a gamma-ray glow that had been ongoing up until that TGF occurred. Another strike caught on camera to the same tower on the same day occurred after a glow had terminated and produced no TGF (Smith et al., 2018).

One of the shortcomings of GODOT was its susceptibility to electrical noise, especially from the power supply at the location where it was hosted in Uchinada. While the PMT produces pulses that all integrate to positive values above baseline, electrical noise is generally random above and below baseline and results in what the detector firmware interprets as many low energy photons. These false events, one of which is shown in figure 15, forced us to develop new criteria for event searches and inspired design changes in THOR (section 4.2).

**LAFTR**

UCSC was part of a collaborative effort to design the Light and Fast TGF Recorder (LAFTR) (Barghi et al., 2017). The goal of LAFTR was to be cheap and light, with the idea of producing many such units to be sent in sounding balloons. Although many of those ballooning projects were cancelled as the pandemic interrupted them in 2020, LAFTR continues to be a possibility for future deployments.

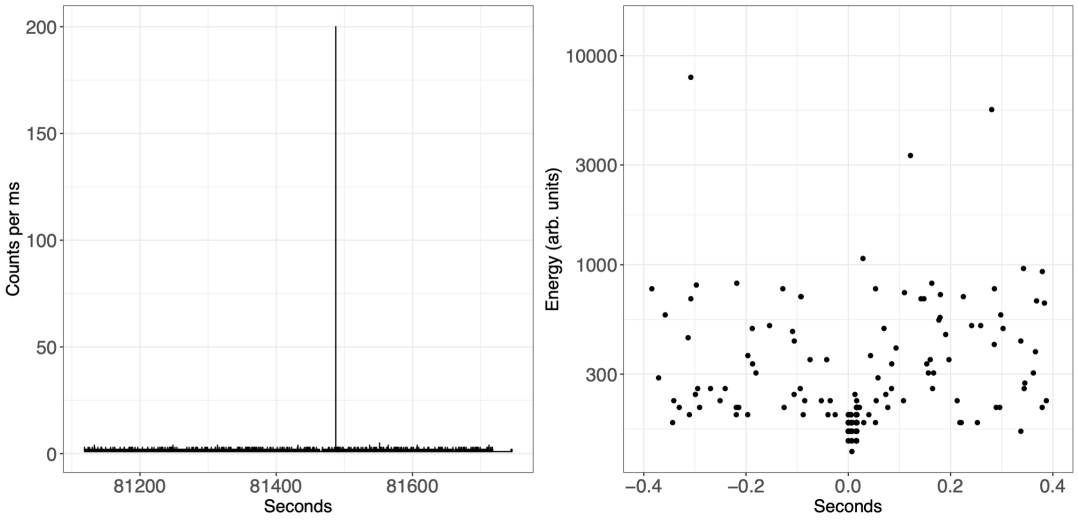


Figure 15: (left) GODOT was plagued with many events like this that appear like a TGF when doing a broad search for bursts on ms time scales. (right) Upon further examination, bursts like these were found to occur at extremely low energies without any associated to lightning activity, and were determined to be caused by RF noise interfering with the electronics.

## 4.2 THOR

In 2018 we began work designing an array known as the "THOR" detector with a grant from the Air Force Office of Scientific Research (AFOSR). With a budget to make 6 identical instruments, we aimed to implement a number of new features outlined below that would improve on previous iterations of ADELE, LAFTR, and GODOT. These improvements were intended to help address some of the outstanding questions in the field alluded to in chapter 3.

In order to achieve a high dynamic range, as discussed in the beginning of section 4.1, we use 3 different sized (but otherwise identical) plastic scintillators in THOR. The goal is to be able to pick up faint or distant events with the large plastic, to not saturate or paralyze in the brightest events with the small plastic, and to supplement everything in between with the medium plastic. We also include a NaI detector for spectroscopy, as the 511 keV line can at times be seen after TGFs or other high energy phenomena in thunderstorms (Dwyer et al., 2015; Enoto et al., 2017). Figure 16 shows the configuration of the scintillators within the THOR box, and table 2 shows their dimensions.

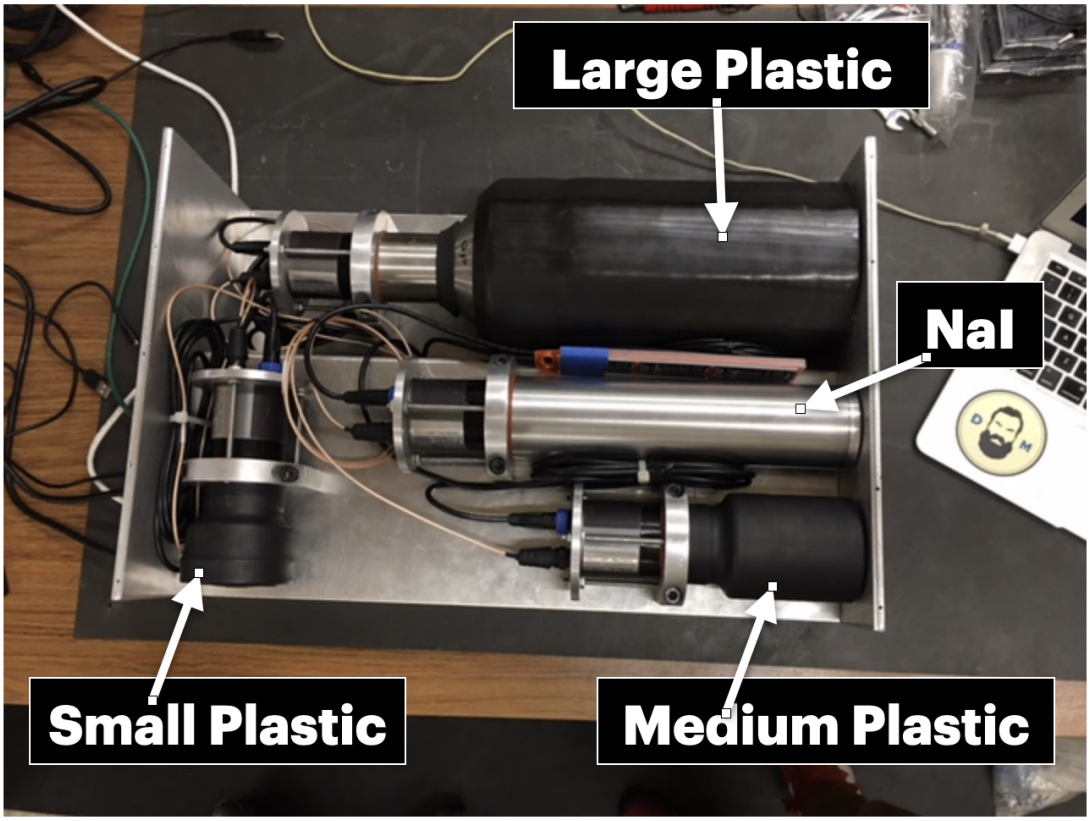


Figure 16: Overhead view of THOR's panel of scintillators.

| Scintillator | Dimensions | Readout |
|---|---|---|
| Small Plastic (Spl) | 1" x 1" x 0.4" block | 3" PMT |
| Medium Plastic (Mpl) | 3" D x 2.25" L cylinder | 3" PMT |
| Large Plastic (Lpl) | 6" x 4.5" x 8.5" block | 5" PMT |
| Sodium Iodide (NaI) | 2" D x 5" L cylinder | 2" PMT |

Table 2: Scintillators in THOR

**Trace and Supplementary Data**

As with most gamma-ray instruments, the output for each of the detectors in THOR is an analog voltage pulse. The instrument must be left on continuously in hopes of capturing a TGF, and even after digitizing the pulse it would take too much memory and processing power to store it on a hard drive. The common solution to this problem is to integrate any pulse above

a set threshold into a single event where the integrated value represents (in theory) the photon's energy.

This works great when the temporal spacing between photons allows for well defined pulses, but at high count rates the pulse from a second photon can enter the integration window of the first. Thus two photons will appear as one photon with the sum of their energy, and if the voltage doesn't drop below baseline by the time the integration window is over (300 ns for THOR), then ensuing photons will continue to "pile up" and appear as a single event.

To help mitigate this problem, we worked with Bridgeport Instruments, the manufacturer of THOR's multichannel analyzer (MCA), to develop a mechanism to save this raw digital waveform for up to 300 µs if the correct trigger conditions are met. We call this raw digital waveform data "trace" mode, and the normal data collection that converts waveforms into individual photon events "list" mode.

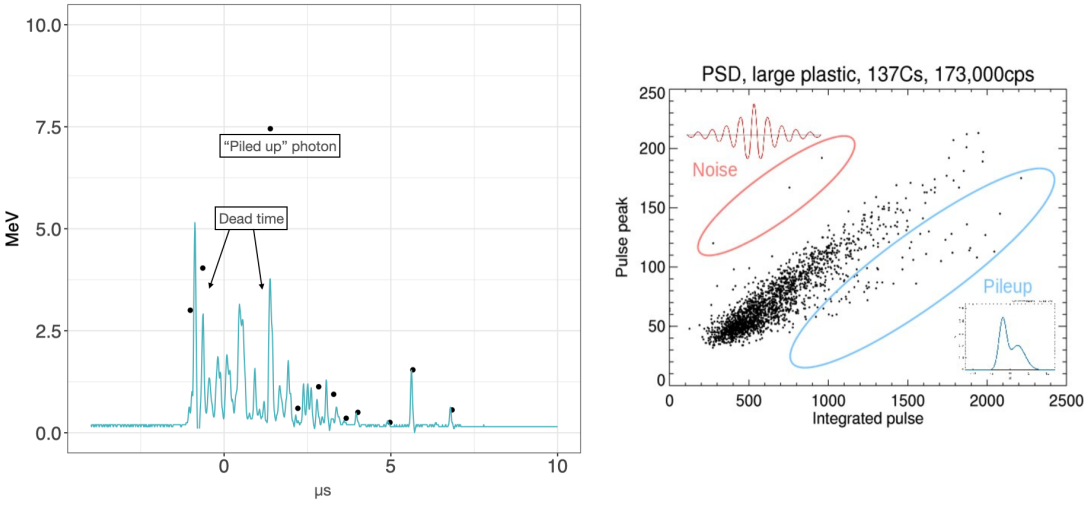


Figure 17: (left) "Trace" mode data (arbitrary units), shown by the blue line, is the digitized voltage pulse coming out of the PMT. Individual photon events are shown as black points in MeV. The energy of the piled up photon is actual an integral of the voltage trace during dead time; many lower energy photons appear as one higher energy photon. (right) For all photons we save the peak value during the integration window, from which we can often infer if any list mode event was due to noise or pileup in lieu of full trace data.

Additionally, the firmware saves the peak value of the trace associated with each photon in

"list mode" for additional information when trace data is not available. The pulse shape for a single photon is well defined, so for each pulse "peak" there will be an expected total value in the integration window. If, for example, a second identical photon enters during that integration window, the peak value will be only slightly higher but the integrated value will double. For this reason, an unusually high integral:peak ratio (points on the bottom right of the rightmost plot in Figure 17) is indicative of pileup. Electrical noise, on the other hand, is generally bipolar in nature so the integral:peak ratio will be lower than usual (represented on the top left of the same plot).

**RF Sealing**

An example of electrical noise creating a false positive is shown in figure 15, but all previous instruments have had issues with noise not only creating false positives but potentially also degrading data of real events. While disturbances in a power supply can happen at any time, lightning will (obviously) also bring a lot of RF noise with it so that the potential for noise coinciding with real events is greater the closer the TGF associated lightning activity is.

The voltage pulses created in THOR are on the order of 100 ns (a product of its previously mentioned plastic/NaI scintillators and Bridgeport PMTs/MCAs), and therefore radiation around 10 MHz will create the most undesirable interference. Using an aluminum composition with a skin depth of a minimum of 80 µm for frequencies 100 kHz and above, and a copper gasket to complete a conductive seal for the box, any RF radiation incident on the box attenuates to insignificant levels. The effect of sealing the box on a typical real photon's pulse is shown in figure 18. An external power filter is used when possible, as noise can still enter the box if attached to a noisy source. This filter is not contained within the box due to space, noise (electrical), and temperature concerns.

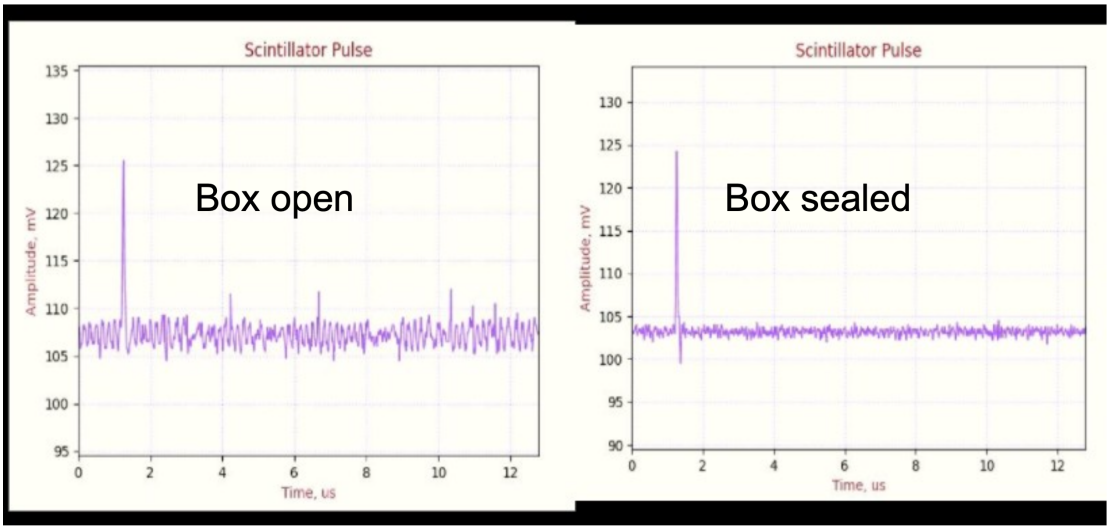


Figure 18: Courtesy David Smith

**GPS Synchronization for µs Timing Accuracy**

Computers can usually achieve at best ms timing accuracy if connected to NTP time servers, and even that accuracy will get blurred out by the uncertainty in the communication between the detector and the computer. Since many processes throughout a lightning flash are on the order of 10s of µs or less (as mentioned in section 3.2), this level of precision will generally not allow for associating gamma-ray activity with those processes. Figure 19 illustrates the importance of synchronizing the photon arrival time within the timescale of features seen in the LF waveforms.

The solution in THOR is to use a GPS receiver that communicates directly to each detector independently. This required the development of a "GPS splitter" inside the box that can split the GPS signal into separate cables going into each detector *without* loss of signal strength or increase in pulse risetime. A triaxial cable is used for the GPS signal to minimize noise inside the box, with the outer coaxial shield grounded to the box.

The GPS signal delivers a pulse at each integer second in UTC time which is read in by the detectors as a photon event with a special boolean flag. The clock in each detector runs at 80 MHz so that each clock "tick" is approximately 12.5 ns. Clock ticks with GPS flags are taken to be true UTC integer seconds, and the durations of each tick between GPS ticks are stretched or compressed slightly (usually less than 0.002%) to match.

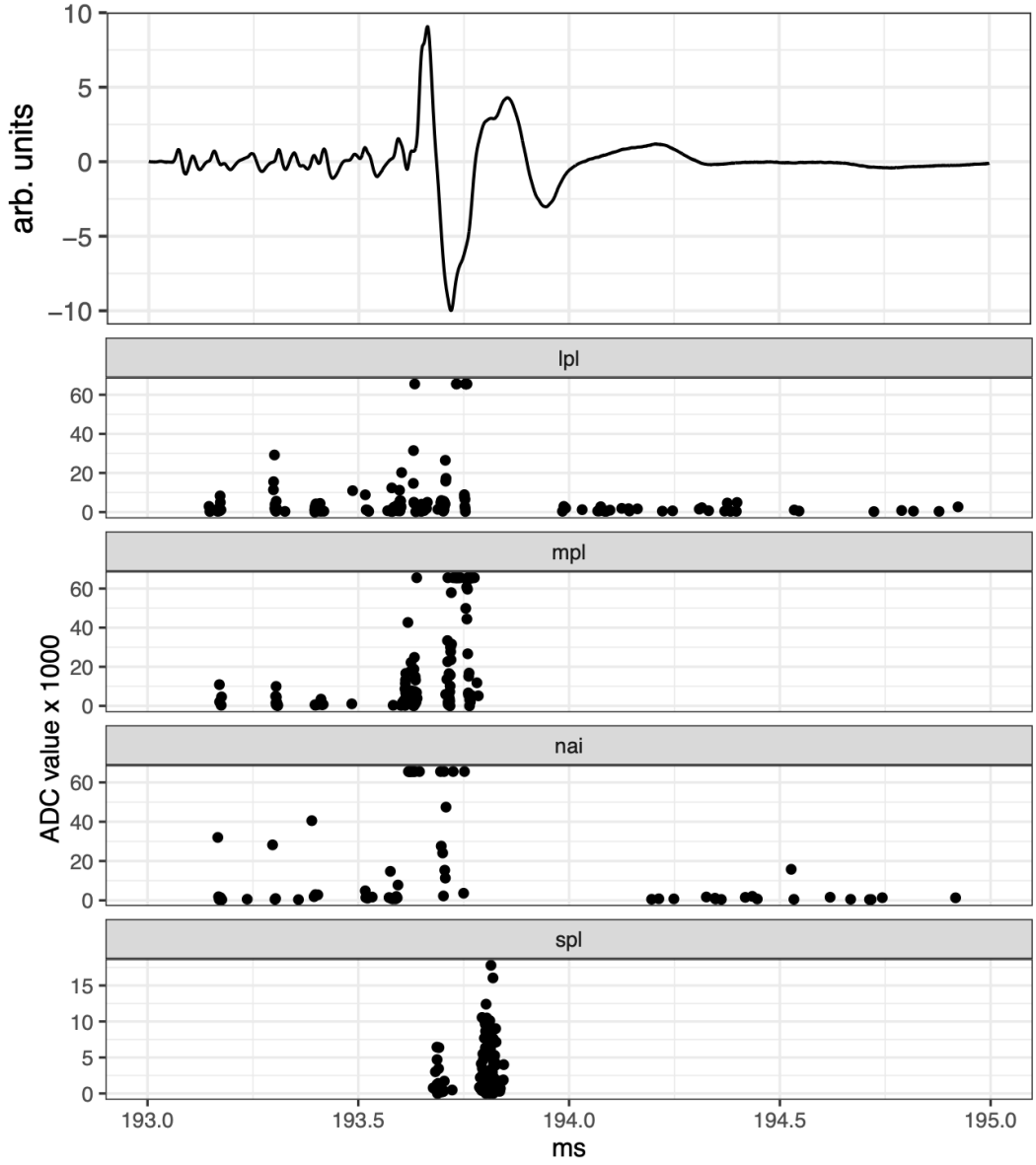


Figure 19: This event from 2022 on Mt. Fuji shows photons in each of THORs detectors in the bottom plots and the LF waveform recorded by Gifu University on top. The µs absolute timing accuracy on THOR allows us for the first time to connect the photons' arrival times with the features of the radio emissions from a lightning flash.

**High Dynamic Range**

Many of the TGFs we see at the ground have a duration on the order of 10s of µs, but THOR

has a deadtime interval of 312.5 ns which yields a theoretical maximum output count rate of 3.2 counts per µs that drops to a maximum output of around 2 counts per µs in a Poisson process. Realistically, we begin to lose significant information due to pileup at above a natural count rate of 1 count per µs although if a trace buffer is saved from an event we can recover some of that lost information up to a point. Above 10 natural counts per µs, we begin to lose virtually all information due to complete paralysis of the electronics.

This means that for a 100 µs TGF, our detectors reach the upper limit of their ideal count rate at 100 total natural counts, and may record nothing at all for an event above 1000 natural counts. Depending on the location, background radiation (also a Poisson process) of 2-3 counts in a 100 µs window is not improbable. If only short windows during nearby lightning activity are searched, then 2 counts may be significant. Thus, in the best case scenario, a range of 2-100 natural counts is ideal for any given detector in THOR, and up to 1000 natural counts will be "detectable" before paralysis.

Being able to detect a minimum of 2 and maximum of 100 counts leaves us with a "dynamic range" of 50 for the count rate $R$, which is much too low for the range of brightnesses of actual events we expect THOR to see. We chose 3 sizes of plastic scintillators in each array to achieve a dynamic range on the order of $10^4$ or more.

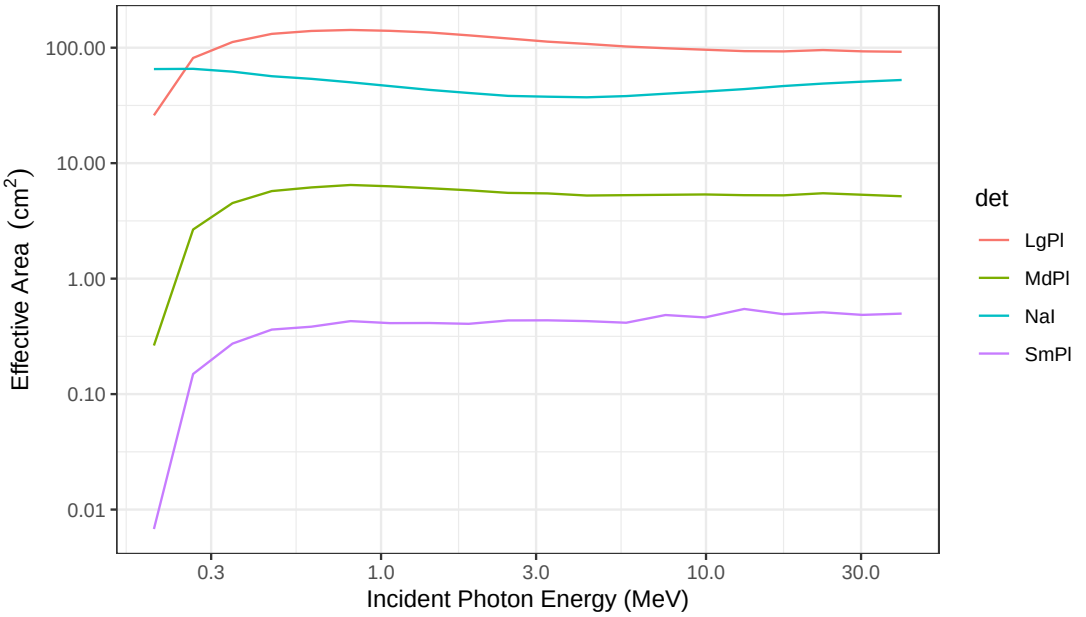


Figure 20: Effective Area by detector in THOR as a function of incident photon energy, as modeled by Geant4

For photons incident on the detectors from a standard TGF spectrum, the effective areas are $A_{\text{eff}} = 0.35, 10.5,$ and $110\text{cm}^2$ for the small, medium, and large detectors respectively (full spectrum shown in figure 20). If we accept that the detectors will be well behaved from 2-100 counts in a 100 µs TGF, then the small plastic will respond well up to $\frac{100}{0.35} = 285.7\frac{\text{counts}}{\text{cm}^2}$ while the large plastic will be sensitive to fluences as low as $\frac{3}{110} = 0.027\frac{\text{counts}}{\text{cm}^2}$ for a total dynamic range of about $10^4$, or $10^5$ if you're willing to accept significant deadtime without paralysis.

## 4.3 Geant4 Simulations for TGF Geometry and Detector Response Curves

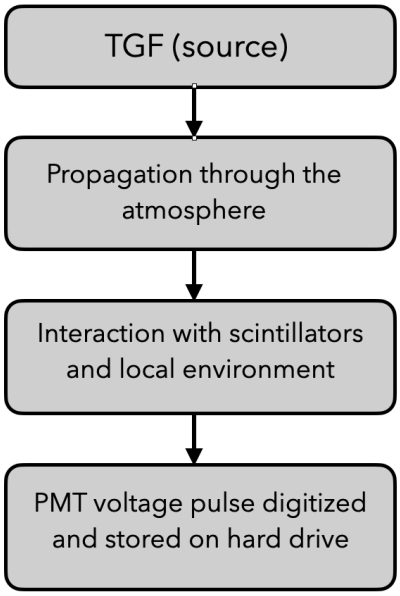


Figure 21: Summary of the chain of events that separate our observations in THOR from the source of the TGF itself that must be simulated/modeled

No matter how good the data quality is at THOR, information on what occurred at the TGF source has been obfuscated or lost through various processes through the atmosphere, local environment near the detector, and the electronics chain of the detector itself as visualized in figure 21. We use CERN's GEometry ANd Tracking (GEANT4) platform (GEANT Team, 1993) to perform Monte Carlo simulations of events in order to get the best range of possible source parameters that are consistent with our observations.

Bowers et al. (2018) built a 3 staged approach to simulating a TGF and its interaction with a detector on the ground that provides the framework for how we model events for THOR:

1. Using (and sometimes modifying) the photon list from Dwyer (2012) as input, allow the photons to propagate through the atmosphere as defined by UsS (1976) until they reach the ground (or desired altitude).

2. Allow the photons saved at stage 1 to interact with the environment surrounding the

detector, saving the photons that are incident on the detector box. This stage may be more or less necessary depending on the environment and whether or not neutrons were seen.

3. Record the energy deposits in each detector from the photons incident on the box.

As mentioned in 4.2, the response of the electronics chain to photon deposits in the scintillators may not be straightforward especially if the count rate is high. This requires an additional set of simulations where the voltage pulses, which have a well known shape that scales with energy, are superimposed on each other to recreate the data we would see stored on THOR's hard drive. An example of this is shown in section 33.

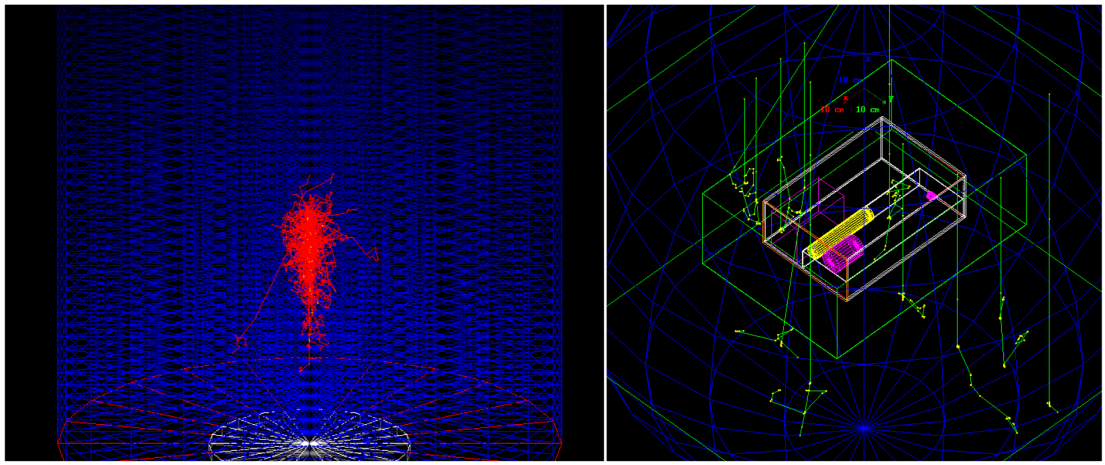

Figure 22: Visualization of Geant4 simulations of (left) photons from a 10 km TGF propagating through the atmosphere and (right) photons interacting with the scintillators inside the THOR detector box

# 5 Detecting an Upward Terrestrial Gamma-Ray Flash from its Reverse Positron Beam

Coauthors: David Smith, Joseph Li, Joseph Dwyer, Gregory Bowers

*The following is a paper that has been published at* https://doi.org/10.1029/2019JD030942 *and is presented in this work verbatim, with the exception of figure numbers adjusted for continuity.*

## 5.1 Background & Summary

Terrestrial gamma-ray flashes (TGFs) are extremely short, intense bursts of gamma rays caused by an avalanche of electrons accelerated to relativistic speeds inside thunderclouds (and coincident with lightning). TGFs were first detected via satellite on the Compton Gamma-Ray Observatory's Burst And Transient Source Experiment (Fishman et al., 1994a), where they stood out as being being brighter than all other gamma-ray activity on Earth combined (Fishman et al., 2011; Dwyer et al., 2010). In addition to the insight TGFs provide into the activity and fields inside thunderstorms, they are of interest to the community because of their potential to deliver dangerous doses of radiation. Dwyer et al. (2010) calculated that a pilot flying above the avalanche region of a TGF could receive a dose equivalent to up to 400 chest X-rays (0.03 Sv).

### 5.1.1 Positron Production inside the Avalanche Region

Inside the source region of a TGF, the electric field is strong enough to overpower the drag force on high energy electrons and accelerate them until they approach the speed of light (Wilson, 1925). These electrons quickly gain enough energy to occasionally knock other (bound) electrons free at relativistic energies in a chain reaction (Gurevich et al., 1992b) that can result in the initial electrons multiplying in number on the order of up to $10^5$ (known as the *avalanche multiplication factor*) (Dwyer, 2008,0). That phenomenon, which is not exclusive to TGFs, is known as a relativistic runaway electron avalanche (RREA). The gamma rays produced by the bremsstrahlung of these electrons (mostly toward the end of the avalanche region) reach very high energies ($\gg$ 1 MeV) and will therefore produce positron/electron pairs on occasion. This pair production is significant; if it occurs within the high-field region, the new positron will be

accelerated to relativistic speeds in the opposite direction.

Since there are no bound positrons to be knocked out of an atom, positrons do not multiply by avalanching the way electrons do. Each time an electron undergoes Møller scattering it not only loses energy itself, but also introduces a new electron, energetic enough to run away but much less energetic than the evolved runaway population. Therefore the positrons and their associated bremsstrahlung gammas have a higher average energy after being accelerated the entire length of the avalanche region, even though there are far fewer of them relative to the electrons. This results in not only higher-energy bremsstrahlung photons, but a more efficient conversion of the particle energy to bremsstrahlung radiation relative to ionization losses. The net result is that the reverse beam has about 1% of the number of gamma-rays in the main, forward beam. The spectra of the two beams are compared in Figure 23.

### 5.1.2 TGF Detection

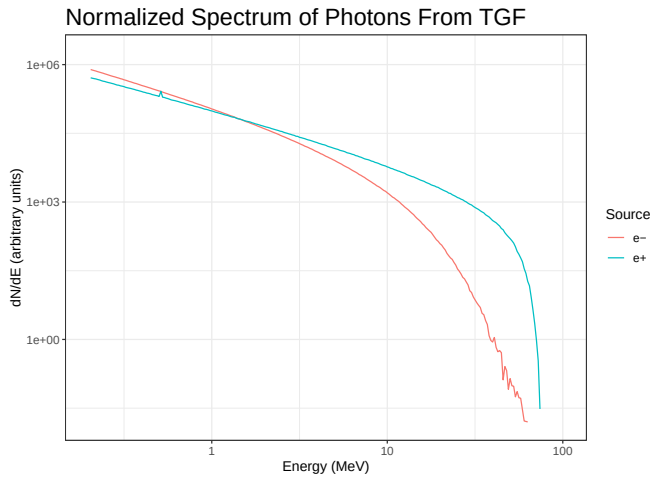


Figure 23: The spectrum of gammas created by positrons from a TGF is slightly harder than the spectrum created by electrons in the 100 keV to 100 MeV range plotted here. Each spectrum is normalized to have the same total number of photons - note that in a TGF there about 100 times as many photons created by electrons as positrons.

On the order of 1,000 upward-directed TGFs occur per day that could be visible by satellite (Briggs et al., 2013), and possibly more if an undetected population of slightly fainter ones exists (Albrechtsen et al., 2019). An estimate for the frequency of downward-directed TGFs does not

exist. Only a handful have ever been detected on the ground if that definition is restricted to events believed to be fully as bright as TGFs seen from orbit, and these events have mostly been associated with upward leaders from rocket wires or towers (Dwyer et al., 2004; Hare et al., 2016; Bowers et al., 2017; Enoto et al., 2017; Wada et al., 2019b). But thousands of upward directed TGFs, which generally occur at altitudes of around 10–15 km (Dwyer and Smith, 2005; Stanley et al., 2006a; Shao et al., 2010; Lu et al., 2010; Cummer et al., 2014,0), have been detected by satellites (Fishman et al., 1994a; Grefenstette et al., 2009; Briggs et al., 2013; Gjesteland et al., 2014; Marisaldi et al., 2014; Østgaard et al., 2019). They produce on the order of $10^{16} - 10^{17}$ upward bremsstrahlung gammas above 1 MeV from electrons (Dwyer and Smith, 2005). And while there are generally 1000 times as many electrons as positrons in a TGF source, positrons produce about 10 times as many gammas in this process as a result of having higher average energy and traveling larger distances on average than the runaway electrons, according to the Relativistic Electron Avalanche Mode (REAM) simulation code of Dwyer (2003). Additionally, the gammas produced by the positrons having a slightly harder spectrum (as seen in Figure 23) results in less Compton scattering in the atmosphere. For this reason, the detectability of the reverse beam at a given amount of intervening atmosphere should be better than the 1:100 gamma-ray ratio relative to the upward beam implies. In this paper, we investigate if the decreased brightness of the downward beam could be offset not only by this effect but by the fact that a detector on the ground would be much closer to the source.

### 5.1.3 Reverse Beam Detection Suspected in Hurricane Patricia

The idea that a TGF could have a reverse beam due to positron bremsstrahlung has been known to be possible in theory given the simulations presented in Dwyer (2008), though the feasibility of detecting such a reverse beam has not been explored in detail. Recently Bowers et al. (2018) believe they observed this phenomenon in the eyewall of Hurricane Patricia in the 2015 season. A TGF was detected onboard an aircraft at 2.6 km altitude, but the radio signal for the associated lightning strike suggested an upward motion of electrons (and therefore upward directed TGF). The intensity of the reverse bremsstrahlung beam observed was consistent with a model of a TGF that would have had an ordinary luminosity if observed from above from space. The observed spectrum was consistent with both a direct and reverse TGF bremsstrahlung beam due to limited photon counting statistics.

## 5.2 Methods

REAM is a Monte Carlo simulation of the avalanche region of an electric field in the air (Dwyer, 2003; Dwyer and Smith, 2005). Seed electrons of the RREA spectrum $\exp(-\frac{E}{7.3MeV})$ are injected into a high field region of 7 avalanche lengths. For a 12 km TGF with $\vec{E} = -400\frac{kV}{m}\hat{z}$, this is a length of approximately 400 meters.

We chose a "standard" TGF for our calculations as one producing $1 \times 10^{17}$ gamma-rays of energy >1 MeV in the primary (upward) beam. This corresponds to $3 \times 10^{17}$ relativistic electrons in the avalanches according to the REAM code (Dwyer et al., 2017) assuming an electric field in the avalanche region of 400 kV/m sea level equivalent. Mailyan et al. (2016) analyzed 40 individual TGFs observed by the *Fermi* spacecraft and found, using the same REAM model, numbers of relativistic electrons ranging from $4 \times 10^{16}$ to $3 \times 10^{19}$ electrons, with a median value of around $8 \times 10^{17}$ (Figure 8a of their paper). As this range of values is sensitive to the best-fit production altitudes, we consider our value of $3 \times 10^{17}$ electrons to be suitably conservative for this study. When Mailyan et al. (2016) used a uniform production altitude of 13.6 km, $3 \times 10^{17}$ electrons was close to the minimum number they found in the sample of 40 TGFs (their Figure 8b).

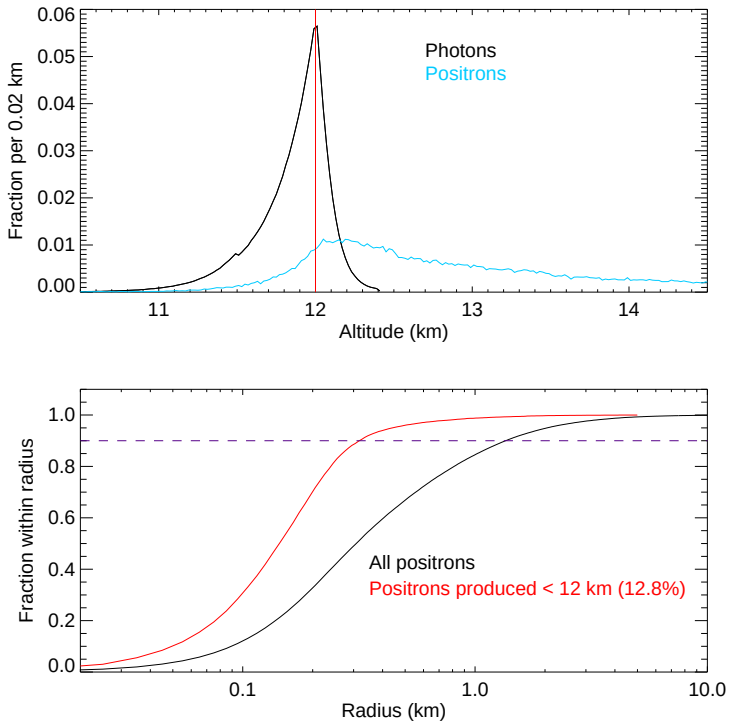


Figure 24: (top) Fraction of positrons and photons produced from an avalanche region extending from 10.4 km to 12 km altitude in REAM. Positrons produced above 12 km will not accelerate in the avalanche region. (bottom) Fraction of positrons created as a function of radial distance from the center of the avalanche. The red line is relevant to the reverse beam as only positrons produced below 12 km have the potential to accelerate downward in the avalanche region. The dashed line indicates 90% of the positron population. In both plots, 'fraction' refers to fraction of total photons/positrons in the simulated TGF.

Positrons are created by bremsstrahlung gammas which are created by the relativistic electrons in the simulation. The output of the simulation for an RREA field region from 10.4 km to 12 km altitude is shown in Figure 24. Though the simulation keeps track of all positrons created, only those within the high field region will contribute to the downward beam — so that any positrons created above 12 km ($\sim 87.2\%$ of the total) can be ignored. The field in the simulation extends infinitely far in the radial direction, so we keep track of the radial distance at which each positron is created. There is no consensus as to the radial extent of the high field region in a TGF, and any positron outside of the high field region will not contribute to the downward beam. However, since $> 95\%$ of all potential runaway positrons are created within a 500 m radius of the avalanche center, any model in which the large-scale thundercloud field reaches the runaway threshold will yield virtually all of the modeled reverse beam.

We save the state of the bremsstrahlung gammas created by the runaway positrons mentioned above. This output includes photon energy, mass thickness ($\frac{g}{cm^2}$) of air traveled from the end of the avalanche region, position in the x-y plane, and the z-component of direction. For the z-component of position, we calculate each photon's altitude from mass thickness of air traveled as if the end of the avalanche region occurred at 8, 10, 12, and 14 km using appropriate air density from the UsS (1976). An azimuthal angle $\phi$ was randomly generated for each photon in our simulation to allow visualization of the detections in the x-y plane (as in Figure 25).

The photons from the REAM output are used as input (with associated position, direction, and energy) in CERN's Geant4 (GEometry ANd Tracking) software for particle physics (Agostinelli et al., 2003; Allison et al., 2016,0). An approximate model of Earth's atmosphere is derived by using 500 m tall slabs of constant density from the UsS (1976) extending from ground level to 20 km. Detection surfaces are placed at 0, 1, 2, 3, and 4 km altitude. While going higher would continue to increase the chance of observing an event, 4 km is a reasonable limit to how high one can expect to find a location able to host a detector (our group recently delivered a detector to the High-Altitude Water Cherenkov Observatory (HAWC) at 4.1 km in southern Mexico (Shao et al., 2018).) EM Opt4, the Geant4 physics list that has the highest priority of accuracy over performance speed, was chosen to ensure accurate modeling in the 100 keV to 100 MeV range (Geant4 Collaboration, 2018).

It is worth noting that there are three primary models for the TGF mechanism. In one, the positrons and X-rays that travel 'upstream' knock enough new electrons free to sustain the

avalanche in a feedback process (Dwyer, 2008,0). The $\vec{E}$-field in this model is relatively uniform in a large volume of space. In the second model, electric field enhancements near lightning leader/streamer tips provide moderately energetic seed electrons that subsequently undergo RREA in the large scale field (Moss et al., 2006; Dwyer, 2008). In both of these models, many positrons are produced by gamma-ray pair production within the region of high field where they can run away, which is the situation we model with REAM. But there are also models in which the seed electrons from the leader tip accelerate and avalanche entirely in a small region of high field around the tip (Moss et al., 2006; Carlson et al., 2009; Celestin and Pasko, 2011). In these models, pair production by gamma rays could occur largely outside the small volume in which the positrons could run away, suppressing the reverse bremsstrahlung beam.

## 5.3 Results

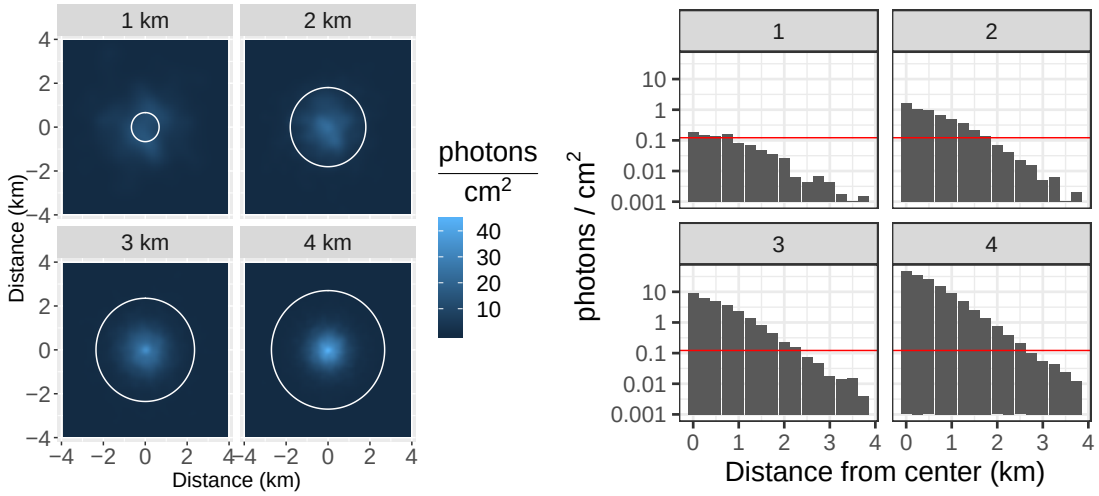


Figure 25: Simulation of a 10 km TGF. (left) Photon density (linear color scale) in the x-y plane at 4 altitudes; the white circles indicate the "radius of detectability". Kernal density estimation (KDE) is used for smoothing. (right) Histogram of fluence/area (logarithmic) vs. distance horizontally from the point beneath a TGF at 10 km – the red line indicates the detectability threshold of 0.12 photons/cm$^2$.

To get a reasonable minimum fluence that would be of interest, we consider a 3 in (7.62cm) diameter by 3 in long NaI detector (3"x 3") looking at energies $> 50$ keV. We modeled such a detector under the average spectrum of the reverse beam at 2 km altitude. The simulation was run under Geant3 (GEANT Team, 1993) using the full mass model for a balloon payload

from the BARREL project (Millan et al., 2013), which includes a NaI detector of this shape, an aluminum frame, some electronics and a styrofoam box – a reasonable stand-in for a generic detector package that might be deployed to a mountain site. The mass model also included a ground surface made of $SiO_2$ underneath the detector package.

This scenario gives a detector effective area of about 49 $cm^2$, 15% of which comes from the detection of photons Compton scattered upwards by the ground. Our 5"x 5" NaI detector at HAWC (4.1 km elevation) receives a background count rate of about 0.2 photons/ms, which translates to 0.072 photons/ms when scaled by area to 3"x 3". Assuming the background follows a Poisson distribution, receiving 6 counts in a millisecond would be expected by chance about once in 63 days. Lightning data could then determine the authenticity of a low count event. Thus we chose 6 counts as a minimum, leading to a fluence threshold of 0.12 photons/$cm^2$ indicated by a horizontal red line in Figure 25. In the event that lightning data were not available and false positives could not be tolerated, a threshold of 8 counts (fluence threshold 0.16 photons/$cm^2$) would give a chance detection once in 2000 years.

The fluence will decrease for a given altitude the farther a detector is horizontally from the point directly under the TGF. Thus we define a "radius of detectability" inside which the fluence will always be above the 6 count threshold for a 3x3" NaI detector. This is best illustrated in the left panel of Figure 25.

For a detector at 4 km, the fluence rises up to a maximum of several hundred photons/$cm^2$. As a TGF normally takes place on the order of $10^{-4}$ seconds (Roberts et al., 2018), the flux at 4 km could be enough to paralyze a detector or at least cause significant dead time.

| Alt. (km) | Radius of Detectability (km) | Area of Detectability ($km^2$) |
|---|---|---|
| 1 | 0.7 | 1.4 |
| 2 | 1.8 | 10.2 |
| 3 | 2.4 | 17.4 |
| 4 | 2.7 | 23.0 |

Table 3: Detectability of a downward 10 km TGF versus observation altitude

The prominent central peak that appears in the 4 km detector in Figure 25 becomes more

diffuse at lower altitudes. The horizontal spreading of the photons due to their angular distribution and the increased likelihood of Compton scattering through additional atmosphere (which gets increasingly dense) both contribute to this effect. Thus the radius of detectability is not solely a function of the intensity of the beam at any given altitude, and has a maximum around 2.5-3 km as seen in Figure 26.

The altitude at which a TGF occurs will have a significant impact on its flux at the surface. Cummer et al. (2014) and Cummer et al. (2015) report 5 TGFs associated with lightning leader tips around 8-12 km (however they do not conclude altitudes for the TGFs themselves). Simulations with TGF source heights at 8, 10, 12, and 14 km (see Figure 26) reveal that TGFs occuring at 14 km and above would not be detectable at altitudes of 1 km and below. The relative prevalence of different source altitudes as a function of location is unknown, however a general correlation with tropopause height is to be expected (Smith et al., 2010).

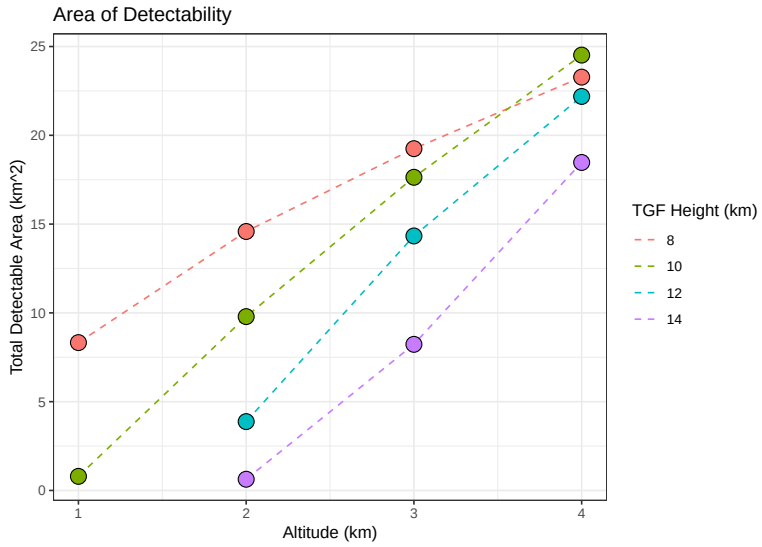


Figure 26: Four lines corresponding to four different TGF source altitudes illustrate the maximum area covered by a detector when placed at different elevations. The points are simulation results and the dotted lines are a simple linear interpolation. For detectable area 10 km$^2$ in a region that averages $0.1\frac{TGF}{km^2 \cdot year}$, the expectation value would be 1 detection per year.

## 5.4 Discussion

Roberts et al. (2018) identified over 1000 TGFs recorded by the Fermi Space Telescope Gamma Ray Burst Monitor that were also located to specific lightning activity by the World-Wide Light-

ning Location Network (WWLLN). In addition to making the location data publicly available [1], they examined the "coastline-distance distribution" and found that locations 0-80 km inland in tropical regions in general have the highest density of TGFs. A similar result was found by Albrechtsen et al. (2019). In general it seems that low-latitude, mountainous ($\geq$ 1 km) regions within 80 km of a coast would make good candidate detector sites.

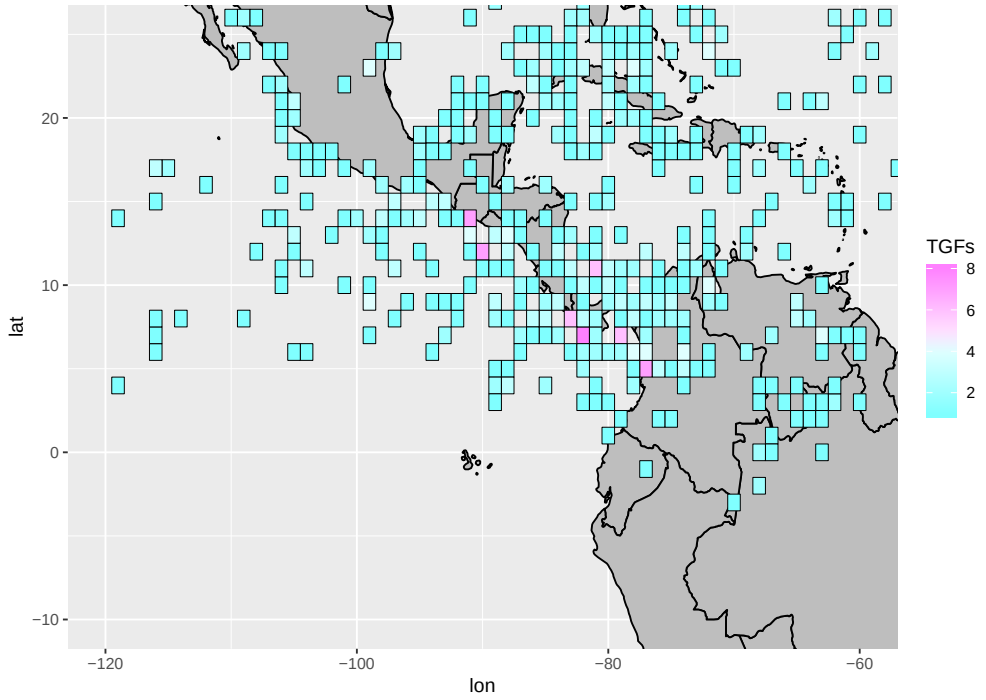


Figure 27: A tiled heat map showing TGFs detected by Fermi/WWLLN per square degree of latitude and longitude in Central America. Although the sample size is small, certain areas appear to be prone to higher TGF activity and could provide a starting point when searching for a candidate detector site.

Searching the Fermi database, as many as 7-8 TGFs per square degree (see Figure 27) were found in some tropical regions over the 6 years of data collection. A rough estimation can be made of $\rho_{tgf}$ (TGF per km$^2$ per year) for such regions. The parameters are broken down as shown in Table 2 and used as in equation 1. TGFs without a WWLLN match were not included in this analysis, as the TGF viewing radius of Fermi GBM (800 km) is much larger than 1 degree at the equator (111 km). It is also important to appreciate that some factors that influence thunderstorm development, such as distance to coastline and local topography, change on the 100 km distance scale.

[1] Fermi Science Support Center; http://fermi.gsfc.nasa.gov/ssc/data/access/gbm/tgf

| Variable | Description | Value |
|---|---|---|
| $\rho_{\text{Fermi}}$ | Density of TGFs per year per $km^2$ detected by Fermi | $1.25 \times 10^{-4} \frac{\text{TGF}}{\text{km}^2 \cdot \text{yr}}$ |
| $f_{\text{livetime}}$ | Fraction of time that a point can be detected by Fermi. This is calculated based on the latitude of these high density regions, given the 25.6° inclination and effective detectability radius of 425 km (Briggs et al., 2013; Smith et al., 2016). The latitudes of the high density regions were between 5° and 12°, leading to less than a 5% variation in $f_{\text{livetime}}$. | $1.7 \times 10^{-3}$ |
| $\eta_{\text{localization}}$ | TGF localization efficiency: a WWLLN match was found for just under 1 in 3 TGFs, so on average there were just over 3 times as many TGFs in each degree than WWLLN matches. | 0.32 |

Table 4: Parameters for calculating local TGF occurrence rates

$$\rho_{\text{tgf}} = \frac{\rho_{\text{Fermi}}}{f_{\text{livetime}} \cdot \eta_{\text{localization}}} = \frac{1.25 \times 10^{-4}}{1.7 \times 10^{-3} \cdot 0.32} \approx 0.2 \frac{\text{TGF}}{\text{km}^2 \cdot \text{yr}} \tag{1}$$

Several detector altitude and TGF source height configurations produce an area of detectability in the tens of $\text{km}^2$, which would suggest an expected detection rate of several reverse beams per year.

## 5.5 Conclusion

Simulations suggest that a detector at an altitude of a few km would see significant counts from the downward positron beam of an upward directed TGF occurring within a few radial km of directly overhead at normal altitudes, with a $> 2$ km detector altitude being suitable for tropical TGFs happening at altitudes up to 14 km. Choosing such a high elevation site with high TGF frequency would be imperative to maximize the odds of making a detection. Further research into TGF source height and frequency by region is planned.

# 6 Detecting Two Laterally Distant TGFs in Uchinada, Japan

Coauthors: David Smith, Masashi Kamogawa, Joseph Dwyer, Gregory Bowers, Jeffrey Chaffin, Jeff Lapierre, Daohong Wang, Ting Wu, Tomoyuki Suzuki

*Note: The following is a paper that has been submitted to the Journal of Geophysical Research and is undergoing review at the time of this work. Figure numbers have been updated for continuity.*

## 6.1 Background

Terrestrial gamma-ray flashes (TGFs) are extremely short, intense bursts of gamma rays caused by an avalanche of electrons accelerated to relativistic speeds inside thunderclouds (and coincident with lightning). TGFs were first detected via satellite on the Compton Gamma-Ray Observatory's Burst And Transient Source Experiment (Fishman et al., 1994a), where they stood out as being bright enough to saturate typical gamma-ray detectors at a distance of 600km away. (Fishman et al., 2011; Dwyer et al., 2010). In addition to the insight TGFs provide into the activity and fields inside thunderstorms, they are of interest to the community because of their potential to deliver dangerous doses of radiation. Dwyer et al. (2010) and Pallu et al. (2021) have calculated that a pilot flying above the avalanche region of a TGF could receive a dose equivalent to up to 400 chest X-rays ($> 0.02$ Sv).

### 6.1.1 Ground Detections of TGFs

While thousands of TGFs have been detected by satellite, only a few have been detected from the Earth's surface. Several of those were recorded in Florida, by both naturally occuring lightning (Dwyer et al., 2012; Tran et al., 2015) and triggered lightning flashes (Dwyer, 2004; Hare et al., 2016). Wada et al. (2022) report on 7 TGFs recorded throughout a multiyear campaign in Kashiwazaki and Kanazawa on the west coast of Japan, and a total of 5 TGFs have been detected in nearby Uchinada, Japan (Bowers et al., 2017; Smith et al., 2018). These ground instruments have provided the first confirmation of TGFs associated with cloud-to-ground (CG) lightning flashes, and direct evidence of the photonuclear reactions induced by the high energy gammas in a TGF (Enoto et al., 2017; Bowers et al., 2017).

### 6.1.2 Constraining the Beam Angle of TGFs

The majority of the photons in a TGF are created through a phenomenon known as relativistic runaway electron avalanches (RREA), where the strength of the background electric field is stronger than the drag force on electrons (above a certain energy threshold) in air (Wilson, 1925). This large RREA E-field is about 2 orders of magnitude too weak to accelerate free electrons above that energy threshold, but there are two proposed mechanisms by which such "seed" electrons can be produced: (1) by a feedback process in which each avalanche produces $> 1$ new seed electron (Dwyer, 2012) and (2) a small-scale E-field at the lightning leader tip strong enough to accelerate free electrons above that necessary threshold (Celestin and Pasko, 2011). These are often referred to as the relativistic feedback model and the cold runaway model, respectively.

Although the cold-runaway model ensures the seed electrons have a relatively wide angular distribution, more than 99% of the gamma-rays come from the large RREA region (Carlson et al., 2009). Only in a model where the majority of the TGF is produced by cold runaway would no large RREA field be present, possibly leading to a more divergent beam of gamma rays (Celestin and Pasko, 2011). The angular distribution of each model thus may not always be sharply distinguishable. Dwyer (2012) notes that it is likely the geometry of the field at the *end* of the avalanche region - where most of the photons are produced - that is most responsible for this angular distribution, where the converging of the field lines due to discharge from the runaway electrons can broaden the beam by up to 25 degrees.

With the exception of a few coincident detections between ASIM, AGILE, and Fermi satellites (Marisaldi, 2020), there is an inherent difficulty in obtaining information about a TGF's beam from only one discrete location in its entire footprint. For these single, discrete detections, Monte Carlo simulations are often used to help evaluate the possible parameters behind the TGF that produced the gamma-rays that hit the detector. However, even with good localization of the associated lightning flash from radio waveforms, there will be a large range of initial parameters that reproduce observed data to an acceptable degree. These free parameters include not only the angular distribution, but also TGF intensity, tilt of the beam, some margin of error of the lightning localization itself as well as uncertainty in where exactly the TGF was produced relative to the leader channel.

| Detector | Scintillator | Effective Area ($cm^2$) |
|---|---|---|
| GODOT | Small Plastic (Spl) | 0.47 |
| (2014-Present) | Large Plastic (Lpl) | 49.8 |
| | Sodium Iodide (NaI) | - |
| THOR | Small Plastic (Spl) | 0.24 |
| (2021-Present) | Medium Plastic (Mpl) | 8.60 |
| | Large Plastic (Lpl) | 94.2 |
| | Sodium Iodide (NaI) | 57.2 |

Table 5: Gamma-ray detectors deployed in Uchinada, Japan. Effective area calculated for the spectrum described in section 6.3

Mailyan et al. (2016) simulated 46 TGFs detected by the Fermi Gamma-ray Burst Monitor by varying intrinsic brightness, source altitude, and wide vs. narrow angular distribution models. Most TGFs were consistent with both wide and narrow models, while a few matched only one or the other. Notably, beam tilt was assumed perfectly vertical to prevent the model overfitting the data, and a wide range of intrinsic brightness values had to be allowed. Lindanger et al. (2021) performed similar analysis on 17 TGFs from the Atmosphere-Space Interactions Monitor, again assuming each TGF's orientation was precisely vertical, but now considering 5 discrete Gaussian distributions to define the beam profile. A variety of these distribution, source altitude, and intrinsic brightness values were found to be acceptable, with the best fits generally favoring the wider Gaussian distributions for most TGFs in their data set.

## 6.2 Data Sources

### 6.2.1 Gamma-ray Instruments

Two gamma-ray observing instruments were placed in the town of Uchinada on the west coast of Japan: GODOT (Gamma-ray Observations During Overhead Thunderstorms) (Bowers et al., 2017) and THOR (Terrestrial High-Energy Observations of Radiation). The features and deployment details of each instrument are described in table 5.

## 6.3 Geant4 Simulations

In order to calculate the effective area of each detector and investigate the possible different TGF source geometries, we used CERN's Geant4 (GEometry ANd Tracking) software for particle

tracking (Agostinelli et al., 2003; Allison et al., 2016,0). Details of the full TGF simulations are discussed in section 6.5.2.

Effective area of each detector was calculated by simulating a source of photons just above their surface. The spectrum of those photons was itself calculated from simulations of a 1.5 km altitude TGF. Only photons incident on the ground 2 km or more away from the vertical axis of the TGF were included in this spectrum, so as to more accurately reflect what the detectors saw in these events. This spectrum is slightly softer than what would be seen closer to the vertical axis, as most of the photons had to be Compton scattered to enter this region in the first place.

### 6.3.1 Radio and Optical Observations

Radio observations of the associated flashes were made by Franklin Electric's Japanese Lightning Detection Network (JLDN), Japan Meteorological Agency's LIghtning DEtection Network (LIDEN), Earth Networks Total Lightning Network (ENTLN), and the Fast Antenna Lightning Mapping Array (FALMA)/ Discone Antenna Lightning Mapping Array (DALMA) of Gifu University (Wu et al., 2021b; Wang et al., 2022). Optical observations of the Dec. 18 2020 flash were made by the Lightning Attachment Process and Observation System (LAPOS) (Wang et al., 2013).

FALMA uses LF sensors while the newer DALMA uses VHF. DALMA is therfore better suited for 3-D locating of whole lightning flashes its altitude estimates will be more accurate than that of FALMA.

## 6.4 Observations and Data

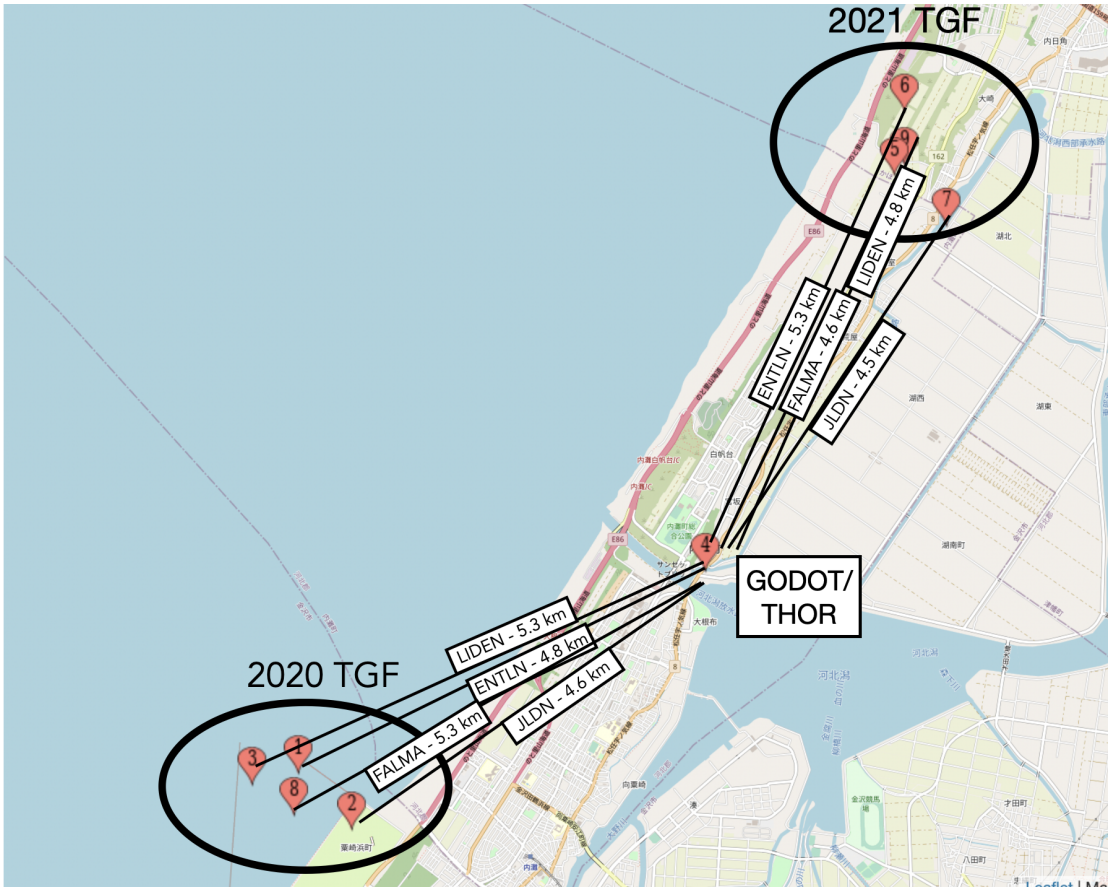


Figure 28: Marker (5) represents the location of GODOT and THOR detectors. (1), (2), and (3) represent the 2020 lightning locations as made by ENTLN, LIDEN, JLDN, and FALMA respectively. (6) and (7) represent the locations of the 2021 flash by FALMA and ENTLN

### 6.4.1 Dec. 18 2020 TGF

In this first TGF, in which only GODOT was active, the large plastic scintillator detected 32 counts in a 30µs window. Its effective area of 48.1 $cm^2$ suggests a lower limit of fluence of around $0.88 \frac{\text{gammas}}{cm^2}$ at the detector site when accounting for the minimal possible effects of dead time (see section 6.4.3). The NaI detector paralyzes too easily due to its long decay time, and the small plastic received too few counts for a reliable extrapolation of the natural count rate.

Data from three separate lightning location networks placed the associated lightning flash

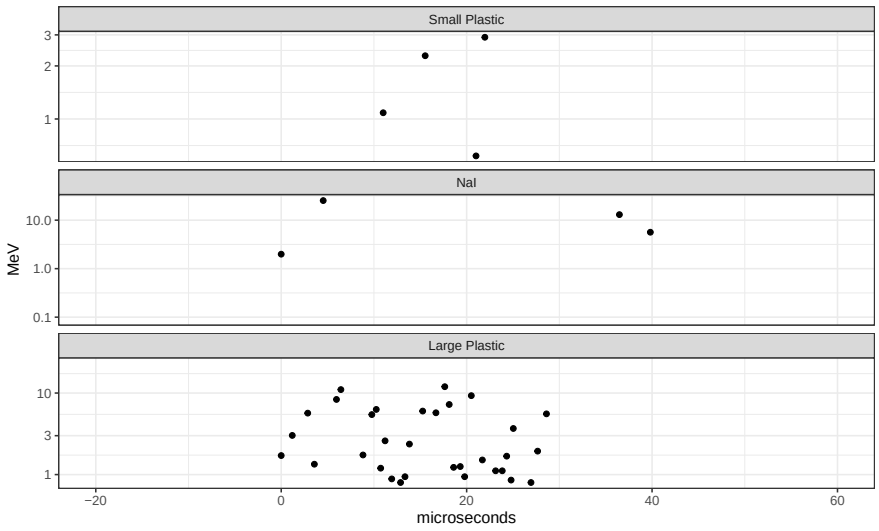


Figure 29: Photons recorded by GODOT. The timing accuracy is on the order of 1 ms, so the x-axes were lined up manually on the assumption that the small plastic (top) detector saw counts during the peak flux, and the NaI detector experienced dead time during the peak.

approximately 5 km from GODOT and 1.5 km or less in altitude (though vertical accuracy was low). The optical sensor from LAPOS also observed the downward leader and ensuing return stroke, as detailed in Wu et al. (2021a). LAPOS made an optical observation of the downward leader emerging from the cloud base at 1.2 km altitude. They also measure the leader's speed, and can extrapolate an upper limit of the its initial height at 1.8 km. GODOT would be greater than **70**° off the vertical axis of a TGF at or below 1.8 km.

The return stroke was notable for its extremely strong current (estimated at −335 kA by FALMA) and smooth bipolar waveform. This particular waveform has been categorized with others like it as a "compact return stroke" (Wu et al., 2021b,0), which has previously been associated with TGFs (Wada et al., 2022).

### 6.4.2 Dec. 18 2021 TGF

The second TGF, occurring exactly a year later, also yielded a modest fluence at the detector site. Both GODOT and THOR were active during this event.

In THOR, the large plastic detector collected 36 counts, which would suggest a minimum of $0.78 \frac{\text{photons}}{\text{cm}^2}$. The medium plastic detector suggested a higher fluence of $2.9 \frac{\text{photons}}{\text{cm}^2}$ with only 22 counts but a much smaller effective area. Since THOR has trace data available (the direct

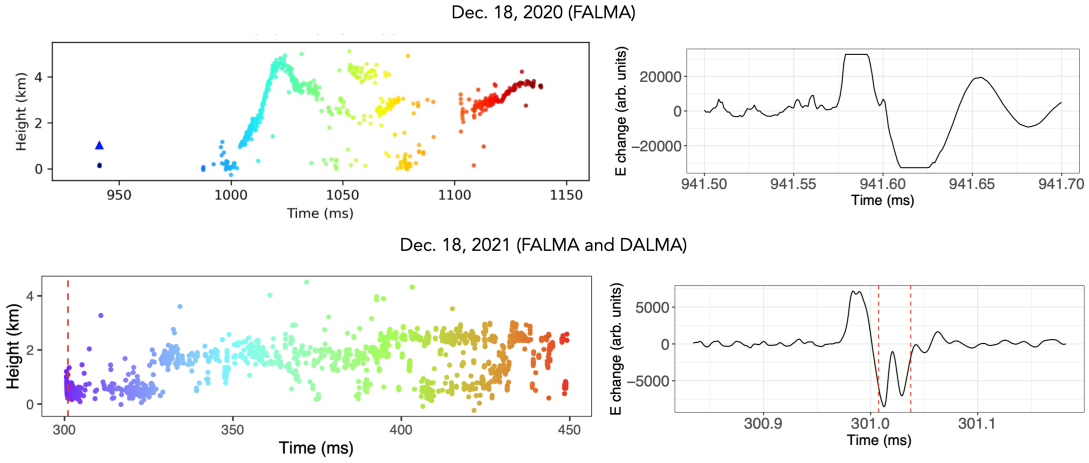


Figure 30: (left) Altitude estimates for all lightning activity provide an upper limit on where a radio silent TGF could have possibly occurred of around 4-5 km. DALMA data in 2021 has higher altitude accuracy. (right) LF waveforms of the return stroke associated with both of the TGFs is classifed by Wu et al. (2021b) as Compact Return Stroke. The timing of the gamma-ray production is indicated at or between the red lines, only available in 2021 when THOR was active.

voltage pulse created by the PMT) we can see that the large plastic detector experienced dead time and pileup and therefore undercounted while the medium plastic experienced minimal dead time. The large plastic detector in GODOT received 26 counts and likely suffered similar deadtime effects, though it does not collect trace data.

Four localizations were made with radio data (see figure 28), however no optical observations were available. The similar lateral flash distance of $\approx 5$ km thus comes with similar confidence to the 2020 event, and DALMA gives a reliable altitude estimate of 1083 m for the approximate top of the return stroke (see figure 30).

It's well documented that winter thunderstorms in Japan are quite low (Yoshida et al., 2019), with cloud tops typically below 6 km and main negative charge centers around 2-3 km altitude, which together with the radio and optical data gives a consistent picture of very low altitude -CG flashes for each event. We use this radio and climatological data to guide the limits of simluated altitudes in section 6.5.2.

Similar to the 2020 event, the associated return stroke was extremely strong (peak current $-238$ kA) and its waveform was again categorized as a compact return stroke.

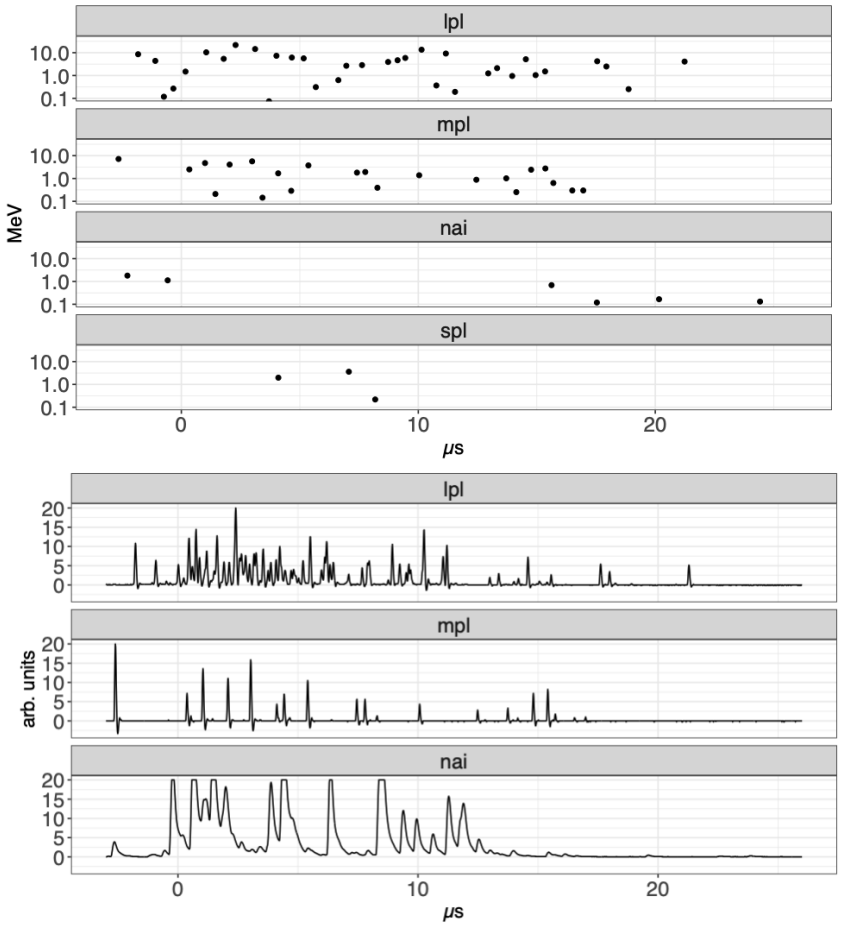


Figure 31: Gamma ray data from the Dec. 18 2021 TGF. In the list mode data in the top chart, each dot represents a photon with a given arrival time and energy. Trace data on the bottom shows direct voltage output from the PMT. List mode data will underestimate total counts for regions where individual pulses aren't easily distinguishable; this is especially obvious during peak intensity in the large plastic and NaI detectors.

### 6.4.3 Dead Time Analysis

Both THOR and GODOT have a programmable deadtime of 312.5 ns, during which any additional incident photons are registered as the same single count. This results in a measured count rate that can be well below the natural count rate especially as the natural count rate increases (as shown in figure 32). THOR allows for a quicker recovery after the 312.5 ns deadtime interval

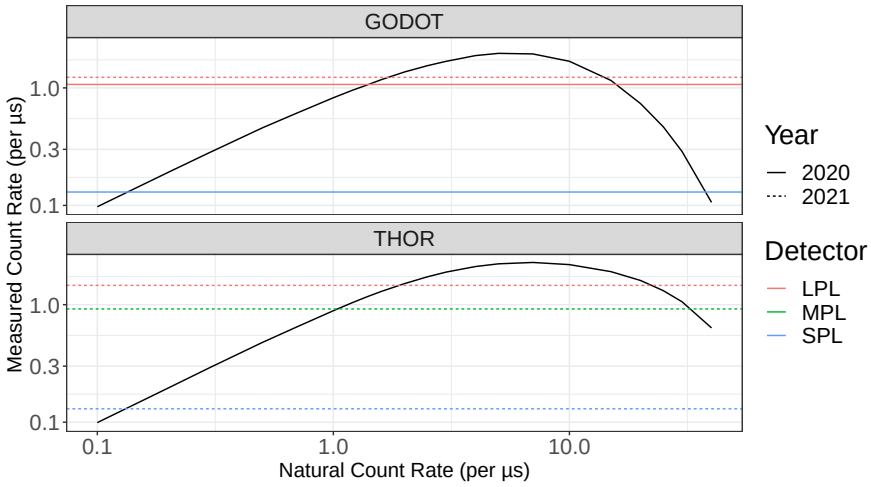


Figure 32: Black curve is the result of simulations of measured vs. actual count rate for the detectors. Horizontal lines represent the average count rate during each of the events in each of the detectors. Above a certain natural count rate, the measured count rate begins to decrease as the effects of dead time take over.

and therefore has a slightly different response curve.

Although the average measured count rate is shown, the natural count rate during a TGF is known to vary with time and therefore its exact reconstruction is not possible through these livetime curves. Additionally, because the measured rate will actually start to decrease as natural rate continues to increase past a certain point, each measured rate has two possible natural count rates. The lower of those two matches for the average count rate provides a lower limit for the natural count rate, which is used in table 6.

If our hypothesis is correct that the discrepancy between the medium and large plastic detectors is due to deadtime, it should be possible to simulate trace data that delivers a similar number of total measured counts as the large plastic but with a natural count rate closer to that of the medium plastic. In figure 33 we simulate our detector/electronics response to 3 different natural count rates using the expected spectrum at ground level. The best match corresponds to a natural fluence of 5.3 $\frac{\text{photons}}{\text{cm}^2}$, which is much closer to the lower limit estimate of 2.9 $\frac{\text{photons}}{\text{cm}^2}$ given by the medium plastic detector.

Any fluence on the order of 1 $\frac{\text{photon}}{\text{cm}^2}$ is much higher than expected given the geometry of these two TGFs, and most of our analysis suggests a value a few times higher than that. We will use this conservative estimate of 1 $\frac{\text{photon}}{\text{cm}^2}$ as a lower limit to compare with simulations in the next section.

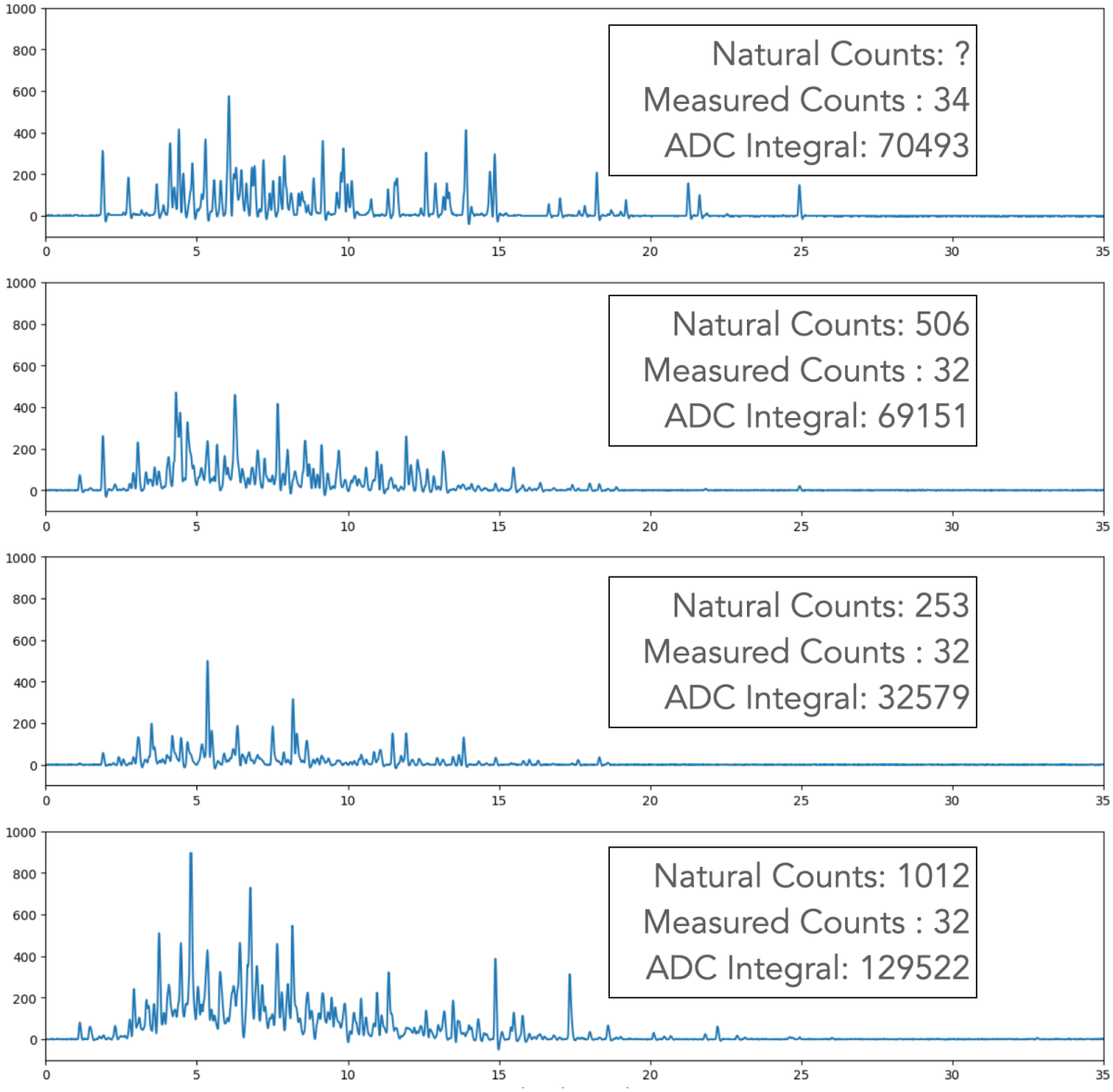


Figure 33: Comparing simulations (bottom three panels) with trace output in the large plastic detector from the 2021 TGF (top panel). The integral of the analog-to-digital conversion of the current pulse (ADC) should not be affected by deadtime (since there was no saturation), and therefore provides a metric for the natural count rate so long as the spectrum is well known.

| | GODOT | | | THOR | | |
|---|---|---|---|---|---|---|
| | Counts | Effective Area ($cm^2$) | Minimum Fluence ($\frac{photons}{cm^2}$) | Counts | Effective Area ($cm^2$) | Minimum Fluence ($\frac{photons}{cm^2}$) |
| Dec. 18, 2020 | | | | | | |
| LPL | 32 | 48.1 | 0.88 | - | - | - |
| MPL | - | - | - | - | - | - |
| SPL | 4 | 0.47 | 8.3 | - | - | - |
| Dec. 18, 2021 | | | | | | |
| LPL | 27 | 48.1 | 0.78 | 36 | 94.2 | 0.50 |
| MPL | - | - | - | 22 | 8.6 | 2.9 |
| SPL | 0 | 0.47 | 0 | 3 | 0.24 | 13.2 |

Table 6: LPL, MPL, and SPL stand for large, medium, and small plastic detectors respectively. Fluences given are the *lower limit* values in $\frac{photons}{cm^2}$ corrected for deadtime based on the average count rate of the TGF. THOR was still in the design phase during 2020.

## 6.5 Analysis

### 6.5.1 Exploring Possible Explanations for Unexpectedly High Fluence

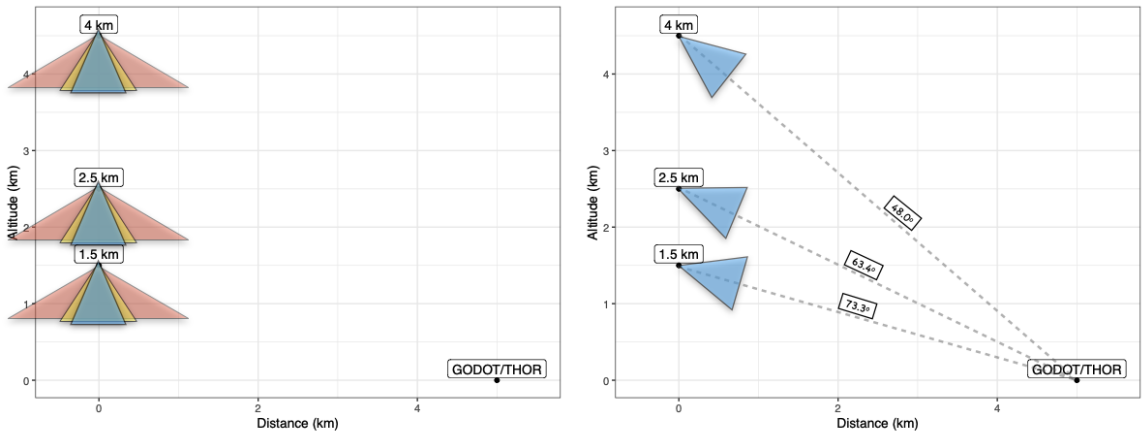


Figure 34: **Left:** Standard (blue cones) vs. wide (yellow ) vs. isotropic (red) beam models each simulated at 3 separate altitudes. The width of each cone represents the opening angle that includes 50% of the TGF's gamma rays (23.5°, 33°, and 60° for normal, wide, and isotropic beams, respectively) **Right:** Tilted beam simulations - the beam was tilted to be directly aimed at the detector arrays to get an upper limit on fluence.

Though other possibilities exist, TGFs are generally thought to occur somewhere along/adjacent to the stepped leader channel (Østgaard et al., 2019; Cummer et al., 2015; Shao et al., 2010). If that were the case for the 2020 TGF with a 0° axis tilt, then GODOT was sitting more than 70° off the axis of the TGF. Since it appears very unlikely to see anything, let alone a flux capable of producing dead time, at such an angle, we explored a number of possible explanations for which to perform Monte Carlo simulations:

- **Unusually Bright**

  Our modeling is all based on a choice of a TGF brightness of $10^{17}$ gammas above 1 MeV, and therefore any resulting fluence that's $X$ times too low can be resolved by assuming the TGF was in fact $X$ times brighter. For comparison, Mailyan et al. (2016) and Lindanger et al. (2021) found the brightest TGFs in their simulation to still fit observations had

$3 \times 10^{19}$ and $1.5 \times 10^{20}$ 'gamma rays at the source', respectively. One particularly bright TGF from the Reuven Ramaty High Energy Solar Spectroscopic Imager (RHESSI) was estimated to have an intrinsic brightness of $3 \times 10^{18}$ gammas. (Gjesteland et al., 2015)

- **A Radio-Silent Upward Propagating Leader**

  A 1.5 km TGF detected 5 km away horizontally would be one of the most extreme "off-axis" detections to date (assuming no tilt). We explore the possibility of a higher TGF leading to more fluence at the detector site by modeling TGFs at 2.5 and 4 km altitude. This is motivated by the fact that FALMA saw lightning activity occuring up to 4 km shortly after the TGF (as seen in figure 30). This would require radio-silent lightning activity at the time of the TGF, which is possible but not likely.

- **Unusually Wide Angular Distribution** In addition to the "normal" beam TGF, we also simulated a TGF where the starting angle of each photon was convolved with a 25° gaussian. For reference, the "wide beam" in Mailyan et al. (2016) contains 75% of all photons in a 36° half-angle cone vs. 45° for ours.

  To test the upper limit of beam widening, we also simulated a standard brightness TGF that was completely isotropic on the bottom hemisphere ($\theta \leq 90°$ with the z-axis pointing down).

- **Conveniently Tilted Axis**

  For each altitude, we also modeled a TGF that was tilted *directly at* GODOT/THOR to get an upper limit on the increased flux that would provide.

### 6.5.2 Geant4 Simulations of the TGF

We used the photon list generated by the Relativistic Electron Avalanche Mode (REAM) simulation code of Dwyer (2003) as input for our simulation (this included separate lists for TGFs of 1.5, 2.5, and 4 km altitude). We then adjusted the angular distribution and/or tilt as outlined above and track the photons propagating through the atmosphere using Geant4.

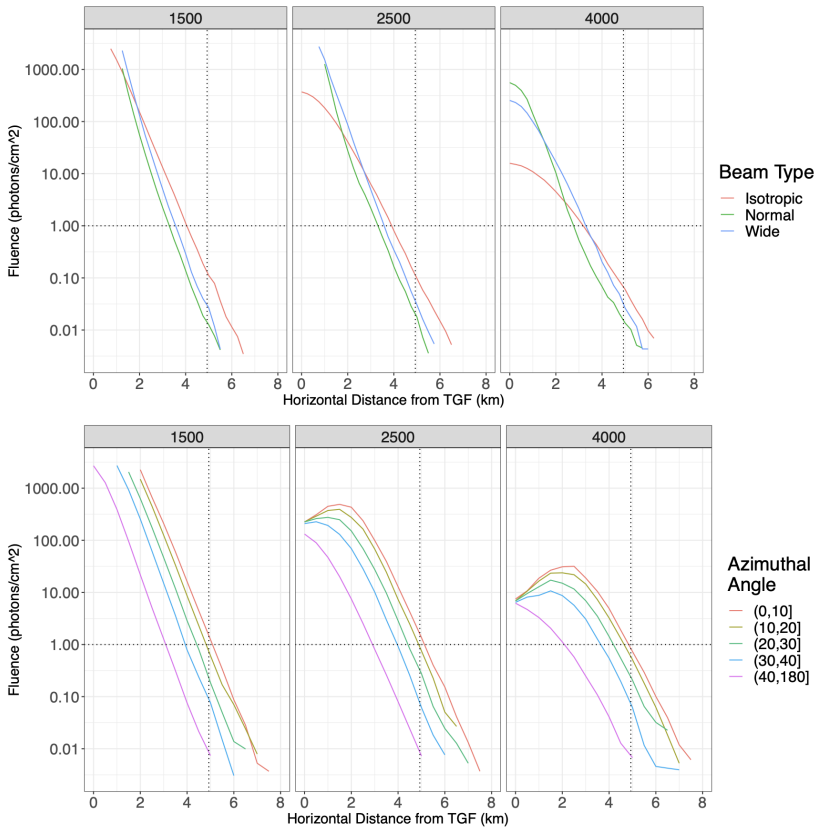


Figure 35: (top) TGF fluence as a function of distance from the center using gammas according to the model in Dwyer (2012), with the colors representing the beam type used. (bottom) Here the colors represent the azimuthal angle from the axis on which the TGF is tilted. (all) The three panels left to right represent a TGF at altitude 1500m, 2500m, and 4000m respectively. The dotted lines represent the best estimate of 5 km distance and lower limit of $1\,\frac{\text{photon}}{\text{cm}^2}$ fluence based on observations.

We found that simulating a "standard" TGF occurring near the top of the leader channel at 1.5 km would produce a fluence of $0.0126\frac{\text{photons}}{\text{cm}^2}$ on the ground 5 km away (range: 0.0041-0.036 $\frac{\text{photons}}{\text{cm}^2}$ from 4.5-5.5 km). As expected, this falls short of the observed fluence by about 2 orders of magnitude. To explain this with "unusual brightness" alone, each TGF would need to have an intrinsic brightness of $10^{19}$ gammas. Possible contributions from other varied parameters are as follows:

**Altitude:**

Contrary to our expectations, increasing the altitude of the simulated TGF had only modest effect on the fluence at large distances. While a higher source altitude leads to a more favorable angle at the detector site, it causes the photons have to travel through more air to get there. Altitudes of 2.5 km and 4 km saw a 41% and 8% increase in fluence at 5 km respectively (using the 1.5 km simulation as basline). Coupled with the radio data's strong support for all lightning activity occuring below 2 km, we consider altitude to be an unlikely factor in either event.

**Beam Width:**

Our wide beam TGF increased fluence by a factor of 2.1, yielding $0.267 \frac{\text{photons}}{\text{cm}^2}$ at 5 km offset with a 1.5 km altitude TGF. The wide beam produced a similarly modest increase in fluence across all altitudes within the 4.5-5.5 km range, so it appears that using a tyical "wide beam" model does not explain our observations either.

The isotropic TGF did at least get within an order of magnitude of our observations, resulting in just over 0.1 $\frac{\text{photons}}{\text{cm}^2}$ at 5 km for 1.5 km and 2.5 km altitudes. However, neither the cold runaway nor feedback models approach such an angular distribution, even in their widest variants. A recently proposed TGF mechanism called "reactor feedback", which involves multiple regions of differently oriented electric fields creating feedback through a reactor-like model, does claim to be able to produce much wider and even quasi-isotropic beams (Stadnichuk et al., 2021).

**Beam Tilt:**

Tilting the beam directly at the detector was the only variation to reach the fluence threshold at standard brightness. In the best case scenario of the nadir angle being that of the TGF origin to the detector distance, the detector needed to be within 20° azimuthally of the TGF axis. While thunderstorms in Japan have been observed to exhibit tilted charge structures due to strong vertical wind shear (Morgenstern et al., 2022).

While this could be explained by these simply being the two of many tilted TGFs that happened to point toward our detectors, radio data would suggest otherwise. Both flashes had a radio pulse identified as a "compact return stroke" as described in Wu et al. (2021b), characterized by their smooth bipolar shape and short duration, and well known to be associated with TGFs. FALMA identified the 2020 and 2021 TGFs as the only two compact return strokes within 5km of GODOT/THOR since 2018.

Even allowing for an equal chance of any tilt angle (i.e. isotropic TGF axis probability

distribution), the chance of 2 TGFs tilting to within the required 20° solid angle of our detector is about 1 in 1100.

**Location Accuracy:**

The location estimates of each stroke range from 4.6-5.3 km from the detector site. On top of that uncertainty, each lightning location network has its own inherent uncertainty on the order of 10s-100s of meters. This is significant because the fluence in our simulations increases by about a factor of 3 (range: 1.9-4.3, depending on beam width and altitude) for each 500m closer to the source. FALMA, which is believed to have the lowest uncertainty of the networks used, locates the 2020 TGF at 5.3 km and the 2021 TGF at 4.6 km.

## 6.6 Conclusion

Monte Carlo simulations suggest two TGFs observed on Dec. 18 2020 and Dec. 18 2021 in Uchinada, Japan, cannot be adequately explained by a "standard" vertically oriented TGF ($10^{17}$ gammas above 1 MeV), leaving a discrepancy of 2 orders of magnitude. Monte Carlo simulations suggest that varying the TGF altitude and beam width are not sufficient to explain the discrepancy, while increasing the brightness by two orders of magnitude or tilting the beam almost horizontally toward the detector are. Further research is warranted into how plausible the latter two scenarios are, or how some more plausible combination of several factors could produce the observed fluence.

# 7 Conclusion and Future Work

## 7.1 Future Work

In addition to the events in Uchinada presented here, THOR has captured multiple additional events that are currently undergoing analysis before being submitted for publication. Several events from July 2022 on Mt. Fuji, one of which is shown in figure 19, are believed to be some of the first events where stepped leader X-ray emissions and a full brightness TGF are observed occurring as part of the same flash (Rakov and Kereszy (2022) previously reported one such event in Florida). Without the accurate GPS timing on THOR, we wouldn't have been able to make the strong temporal connection between those X-ray emissions and individual leader steps.

| Instrument | Location | Motivation |
|---|---|---|
| THOR1 | Telluride, Colorado | Mountaintop Energetic Pulses are common in this region (Lyu et al., 2021) |
| THOR2 | Florida Tech (Melbourne, Fl) | Energetic In-Cloud Pulses (EIPs) common in this region |
| THOR 3 & 6 | LANL (New Mexico) | Frequent summer thunderstorms over the high desert, nearby lightning mapping array and rocketed triggered lightning |
| THOR 4 | Säntis Tower, Switzerland | Frequently struck tower at high altitude, multiple TGFs recorded to date |
| THOR 5 | Uchinada, Japan and Mt. Fuji, Japan | Low winter thunderstorms and high altitude summer thunderstorms; multiple TGFs recorded in both locations to date |
| GODOT | Uchinada, Japan | Placed about a km away from THOR 5 so as to give more infomortation about the spatial variance of fluence at the ground. |

Table 7: THOR and GODOT Deployments

As an added tool to handle extremely bright events, our group is also developing a dosimeter to go inside the THOR box. A dosimeter sacrifices time resolution in order to get an accurate reading of total energy deposited from an event even during extremely high count rates when the other detectors are paralyzed. This can be used to calculate the total counts in an event if you assume to know the energy distribution of the incident photons. The ability to calculate total dose received also gives dosimeters the advantage of being better suited to address questions on the hazard posed by TGFs to human health. Further down the line we hope to add 3-axis RF sensors to our instruments - both of these additions we would promote to other TGF groups as providing valuable supplemental data. The locations of our active detector arrays are given in table 7.

## 7.2 Concluding Remarks

Chapters 5 and 6 both show examples - whether in theory or in reality - of how observations at a distance have the potential to reveal information about what happened at the source of the TGF. Yet in both cases having a single data point in space and time leaves us short of being able to pin down exactly what it is we've learned about he nature of TGFs. A natural response to "we saw this TGF from really far away laterally" would be to say "it turns out TGF beams are (at least sometimes) way wider than we initially thought," yet without a second data point outside of one building in Uchinada, Japan we couldn't conclusively say which variation on the source parameters had the strongest effect on us being able to see it.

In addition to the supplemental use of radio and optical data, the increased capability for concurrent detections between instruments in different locations and collaboration between groups provides a clear path forward for making definitive statements about TGF source parameters. Lindanger et al. (2020) and Mailyan et al. (2016) began this work by comparing Monte Carlo simulations of TGFs with different source parameters to actual observations, but were extremely limited by the degrees of freedom available to match a single data point. Marisaldi et al. (2020) and Colalillo (2021) have both offered preliminary reports of concurrent detections - by 2 or more satellites in the case of the former and on an multi kilometer radius detector array in the latter. New theory papers that have come out since then (Stadnichuk et al., 2021; Pasko et al., 2023; Dwyer, 2021) can provide new insights on possible source conditions. These advances in theory have, not surprisingly, been informed by advances in our understanding of lightning

and streamer physics, a symbiotic relationship we should expect to continue as we develop a complete, scientific theory of thunderstorms that can predict all the possible phenomena they can produce.

# References

(1976). U.S. standard atmosphere. Technical report.

(2000). Intensive x-ray emission bursts during thunderstorms. *Physics Letters A*, 275(1):90–100.

Abarca, S. F., Corbosiero, K. L., and Galarneau Jr., T. J. (2010). An evaluation of the worldwide lightning location network (wwlln) using the national lightning detection network (nldn) as ground truth. *Journal of Geophysical Research: Atmospheres*, 115(D18).

Agostinelli, S., Allison, J., Amako, K., Apostolakis, J., Araujo, H., Arce, P., Asai, M., Axen, D., Banerjee, S., Barrand, G., Behner, F., Bellagamba, L., Boudreau, J., Broglia, L., Brunengo, A., Burkhardt, H., Chauvie, S., Chuma, J., Chytracek, R., Cooperman, G., Cosmo, G., Degtyarenko, P., Dell'Acqua, A., Depaola, G., Dietrich, D., Enami, R., Feliciello, A., Ferguson, C., Fesefeldt, H., Folger, G., Foppiano, F., Forti, A., Garelli, S., Giani, S., Giannitrapani, R., Gibin, D., Gómez Cadenas, J. J., González, I., Gracia Abril, G., Greeniaus, G., Greiner, W., Grichine, V., Grossheim, A., Guatelli, S., Gumplinger, P., Hamatsu, R., Hashimoto, K., Hasui, H., Heikkinen, A., Howard, A., Ivanchenko, V., Johnson, A., Jones, F. W., Kallenbach, J., Kanaya, N., Kawabata, M., Kawabata, Y., Kawaguti, M., Kelner, S., Kent, P., Kimura, A., Kodama, T., Kokoulin, R., Kossov, M., Kurashige, H., Lamanna, E., Lampén, T., Lara, V., Lefebure, V., Lei, F., Liendl, M., Lockman, W., Longo, F., Magni, S., Maire, M., Medernach, E., Minamimoto, K., Mora de Freitas, P., Morita, Y., Murakami, K., Nagamatu, M., Nartallo, R., Nieminen, P., Nishimura, T., Ohtsubo, K., Okamura, M., O'Neale, S., Oohata, Y., Paech, K., Perl, J., Pfeiffer, A., Pia, M. G., Ranjard, F., Rybin, A., Sadilov, S., Di Salvo, E., Santin, G., Sasaki, T., Savvas, N., Sawada, Y., Scherer, S., Sei, S., Sirotenko, V., Smith, D., Starkov, N., Stoecker, H., Sulkimo, J., Takahata, M., Tanaka, S., Tcherniaev, E., Safai Tehrani, E., Tropeano, M., Truscott, P., Uno, H., Urban, L., Urban, P., Verderi, M., Walkden, A., Wander, W., Weber, H., Wellisch, J. P., Wenaus, T., Williams, D. C., Wright, D., Yamada, T., Yoshida, H., Zschiesche, D., and G EANT4 Collaboration (2003). G EANT4—a simulation toolkit. *Nuclear Instruments and Methods in Physics Research A*, 506:250–303.

Albrechtsen, K. H., Østgaard, N., Berge, N., and Gjesteland, T. (2019). Observationally Weak TGFs in the RHESSI Data. *Journal of Geophysical Research (Atmospheres)*, 124:287–298.

Allison, J., Amako, K., Apostolakis, J., Araujo, H., Arce, P., Asai, M., Barrand, G., Capra, R.,

Chauvie, S., Chytracek, R., Cirrone, P., Cooperman, G., Cosmo, G., Cuttone, G., Daquino, G., Donszelmann, M., Dressel, M., Folger, G., Foppiano, F., and Yoshida, H. (2006). Geant4 developments and applications. *IEEE Transactions on Nuclear Science*, 53:270–278.

Allison, J., Amako, K., Apostolakis, J., Arce, P., Asai, M., Aso, T., Bagli, E., Bagulya, A., Banerjee, S., Barrand, G., Beck, B., Bogdanov, A., Brandt, D., Brown, J., Burkhardt, H., Canal, P., Cano-Ott, D., Chauvie, S., Cho, K., Cirrone, G., Cooperman, G., Cortés-Giraldo, M., Cosmo, G., Cuttone, G., Depaola, G., Desorgher, L., Dong, X., Dotti, A., Elvira, V., Folger, G., Francis, Z., Galoyan, A., Garnier, L., Gayer, M., Genser, K., Grichine, V., Guatelli, S., Guèye, P., Gumplinger, P., Howard, A., Hřivnáčová, I., Hwang, S., Incerti, S., Ivanchenko, A., Ivanchenko, V., Jones, F., Jun, S., Kaitaniemi, P., Karakatsanis, N., Karamitros, M., Kelsey, M., Kimura, A., Koi, T., Kurashige, H., Lechner, A., Lee, S., Longo, F., Maire, M., Mancusi, D., Mantero, A., Mendoza, E., Morgan, B., Murakami, K., Nikitina, T., Pandola, L., Paprocki, P., Perl, J., Petrović, I., Pia, M., Pokorski, W., Quesada, J., Raine, M., Reis, M., Ribon, A., Fira, A. R., Romano, F., Russo, G., Santin, G., Sasaki, T., Sawkey, D., Shin, J., Strakovsky, I., Taborda, A., Tanaka, S., Tomé, B., Toshito, T., Tran, H., Truscott, P., Urban, L., Uzhinsky, V., Verbeke, J., Verderi, M., Wendt, B., Wenzel, H., Wright, D., Wright, D., Yamashita, T., Yarba, J., and Yoshida, H. (2016). Recent developments in geant4. *Nuclear Instruments and Methods in Physics Research Section A: Accelerators, Spectrometers, Detectors and Associated Equipment*, 835:186 – 225.

Babich, L., Kutsyk, I., Donskoy, E., and Kudryavtsev, A. (1998). New data on space and time scales of relativistic runaway electron avalanche for thunderstorm environment: Monte carlo calculations. *Physics Letters A*, 245(5):460–470.

Babich, L. P., Kudryavtsev, A. Y., Kudryavtseva, M. L., and Kutsyk, I. M. (2007). Terrestrial gamma-ray flashes and neutron pulses from direct simulations of gigantic upward atmospheric discharge. *Soviet Journal of Experimental and Theoretical Physics Letters*, 85:483–487.

Barghi, M. R., S., Delaney, N., Forouzani, A., Wells, E., Parab, A., Smith, D., Martinez, F., Bowers, G. S., and Sample, J. (2017). Plastic Scintillator Based Detector for Observations of Terrestrial Gamma-ray Flashes. In *AGU Fall Meeting Abstracts*, volume 2017, pages AE33B–2555.

Bowers, G. S., Smith, D. M., Kelley, N. A., Martinez-McKinney, G. F., Cummer, S. A., Dwyer, J. R., Heckman, S., Holzworth, R. H., Marks, F., Reasor, P., Gamache, J., Dunion, J., Richards, T., and Rassoul, H. K. (2018). A Terrestrial Gamma-Ray Flash inside the Eyewall of Hurricane Patricia. *J. Geophys. Res.*, 123.

Bowers, G. S., Smith, D. M., Martinez-McKinney, G. F., Kamogawa, M., Cummer, S. A., Dwyer, J. R., Wang, D., Stock, M., and Kawasaki, Z. (2017). Gamma Ray Signatures of Neutrons From a Terrestrial Gamma Ray Flash. *Geophys. Res. Let.*, 44:10.

Briggs, M. S., Xiong, S., Connaughton, V., Tierney, D., Fitzpatrick, G., Foley, S., Grove, J. E., Chekhtman, A., Gibby, M., Fishman, G. J., McBreen, S., Chaplin, V. L., Guiriec, S., Layden, E., Bhat, P. N., Hughes, M., Greiner, J., Kienlin, A., Kippen, R. M., Meegan, C. A., Paciesas, W. S., Preece, R. D., Wilson-Hodge, C., Holzworth, R. H., and Hutchins, M. L. (2013). Terrestrial gamma-ray flashes in the Fermi era: Improved observations and analysis methods. *Journal of Geophysical Research (Space Physics)*, 118:3805–3830.

Briggs, M. S., Xiong, S., Connaughton, V., Tierney, D., Fitzpatrick, G., Foley, S., Grove, J. E., Chekhtman, A., Gibby, M., Fishman, G. J., McBreen, S., Chaplin, V. L., Guiriec, S., Layden, E., Bhat, P. N., Hughes, M., Greiner, J., Kienlin, A. v., Kippen, R. M., Meegan, C. A., Paciesas, W. S., Preece, R. D., Wilson-Hodge, C., Holzworth, R. H., and Hutchins, M. L. (2013). Terrestrial gamma-ray flashes in the fermi era: Improved observations and analysis methods. *Journal of Geophysical Research: Space Physics*, 118(6):3805–3830.

Brothers, M. D., Bruning, E. C., and Mansell, E. R. (2018). Investigating the relative contributions of charge deposition and turbulence in organizing charge within a thunderstorm. *Journal of the Atmospheric Sciences*, 75(9):3265 – 3284.

Carlson, B. E., Lehtinen, N. G., and Inan, U. S. (2009). Terrestrial gamma ray flash production by lightning current pulses. *Journal of Geophysical Research (Space Physics)*, 114:0.

Carlson, B. E., Lehtinen, N. G., and Inan, U. S. (2010). Terrestrial gamma ray flash production by active lightning leader channels. *Journal of Geophysical Research (Space Physics)*, 115:10324.

Celestin, S. and Pasko, V. P. (2011). Energy and fluxes of thermal runaway electrons produced

by exponential growth of streamers during the stepping of lightning leaders and in transient luminous events. *Journal of Geophysical Research (Space Physics)*, 116:3315.

Chilingarian, A., Hovsepyan, G., and Kozliner, L. (2013). Thunderstorm ground enhancements: Gamma ray differential energy spectra. *Phys. Rev. D*, 88:073001.

Chilingarian, A., Hovsepyan, G., and Kozliner, L. (2013). Thunderstorm ground enhancements: Gamma ray differential energy spectra. *Physical Review D*, 88(7):073001.

Colalillo, R. (2021). *International Cosmic Ray Conference*.

Cooray, V. and Arevalo, L. (2017). Modeling the stepping process of negative lightning stepped leaders. *Atmosphere*, 8:245.

Cummer, S. A., Briggs, M. S., Dwyer, J. R., Xiong, S., Connaughton, V., Fishman, G. J., Lu, G., Lyu, F., and Solanki, R. (2014). The source altitude, electric current, and intrinsic brightness of terrestrial gamma ray flashes. *Geophys. Res. Let.*, 41:8586–8593.

Cummer, S. A., Lyu, F., Briggs, M. S., Fitzpatrick, G., Roberts, O. J., and Dwyer, J. R. (2015). Lightning leader altitude progression in terrestrial gamma-ray flashes. *Geophysical Research Letters*, 42:7792–7798.

Cummer, S. A., Zhai, Y., Hu, W., Smith, D. M., Lopez, L. I., and Stanley, M. A. (2005). Measurement and implications of the relationship between lightning and terrestrial gamma-ray flashes. *Geophys. Res. Let.*, 32:L22804.

Dwyer, J. (2004). Implications of x-ray emission from lightning. *Geophys. Res. Let.*, 31:L12102.

Dwyer, J. R. (2003). A fundamental limit on electric fields in air. *Geophys. Res. Let.*, 30(20):2055.

Dwyer, J. R. (2008). Source mechanisms of terrestrial gamma-ray flashes. *J. Geophys. Res.*, 113:D10103.

Dwyer, J. R. (2012). The relativistic feedback discharge model of terrestrial gamma ray flashes. *Journal of Geophysical Research (Space Physics)*, 117:2308.

Dwyer, J. R. (2021). Terrestrial gamma-ray flashes initiated by positive leaders. *Phys. Rev. D*, 104:043012.

Dwyer, J. R. and Cummer, S. A. (2013). Radio emissions from terrestrial gamma-ray flashes. *Journal of Geophysical Research: Space Physics*, 118(6):3769–3790.

Dwyer, J. R., Liu, N., Eric Grove, J., Rassoul, H., and Smith, D. M. (2017). Characterizing the source properties of terrestrial gamma ray flashes. *Journal of Geophysical Research (Space Physics)*, 122:8915–8932.

Dwyer, J. R., Rassoul, H., Al-Dayeh, M., Caraway, L., Chrest, A., Wright, B., Kozak, E., Jerauld, J., Uman, M., Rakov, V., Jordan, D., Rambo, K., and Smyth, C. (2004). A ground level gamma-ray burst observed in association with rocket-triggered lightning. *Geophys. Res. Let.*, 31:L05119.

Dwyer, J. R., Schaal, M. M., Cramer, E., Arabshahi, S., Liu, N., Rassoul, H. K., Hill, J. D., Jordan, D. M., and Uman, M. A. (2012). Observation of a gamma-ray flash at ground level in association with a cloud-to-ground lightning return stroke. *Journal of Geophysical Research (Space Physics)*, 117:10303.

Dwyer, J. R. and Smith, D. M. (2005). A comparison between Monte Carlo simulations of run-away breakdown and terrestrial gamma-ray flash observations. *Geophys. Res. Let.*, 32:L08811.

Dwyer, J. R., Smith, D. M., Hazelton, B. J., Grefenstette, B. W., Kelley, N. A., Lowell, A. W., Schaal, M. M., and Rassoul, H. K. (2015). Positron clouds within thunderstorms. *Journal of Plasma Physics*, 81(4):475810405.

Dwyer, J. R., Smith, D. M., Uman, M. A., Saleh, Z., Grefenstette, B., Hazelton, B., and Rassoul, H. K. (2010). Estimation of the fluence of high-energy electron bursts produced by thunderclouds and the resulting radiation doses received in aircraft. *J. Geophys. Res.*, 115:D09206.

Enoto, T., Wada, Y., Furuta, Y., Nakazawa, K., Yuasa, T., Okuda, K., Makishima, K., Sato, M., Sato, Y., Nakano, T., Umemoto, D., and Tsuchiya, H. (2017). Photonuclear reactions triggered by lightning discharge. *Nature*, 551:481–484.

Fabró, F., Montanyà, J., Van der Velde, O., Pineda, N., and Williams, E. (2019). On the tgf/lightning ratio asymmetry. *Journal of Geophysical Research: Atmospheres*, 124.

Fishman, G. J., Bhat, P. N., Mallozzi, R., Horack, J. M., Koshut, T., Kouveliotou, C., Pendleton, G. N., Meegan, C. A., Wilson, R. B., Paciesas, W. S., Goodman, S. H., and Christian, H. J. (1994a). Discovery of intense gamma-ray flashes of atmospheric origin. *Science*, 264:1313–1316.

Fishman, G. J., Bhat, P. N., Mallozzi, R., Horack, J. M., Koshut, T., Kouveliotou, C., Pendleton, G. N., Meegan, C. A., Wilson, R. B., Paciesas, W. S., Goodman, S. J., and Christian, H. J. (1994b). Discovery of intense gamma-ray flashes of atmospheric origin. *Science*, 264(5163):1313–1316.

Fishman, G. J., Briggs, M. S., Connaughton, V., Bhat, P. N., Paciesas, W. S., von Kienlin, A., Wilson-Hodge, C., Kippen, R. M., Preece, R., Meegan, C. A., and Greiner, J. (2011). Temporal properties of the terrestrial gamma-ray flashes from the Gamma-Ray Burst Monitor on the Fermi Observatory. *Journal of Geophysical Research (Space Physics)*, 116:A07304.

Fuschino, F., Marisaldi, M., Labanti, C., Barbiellini, G., Del Monte, E., Bulgarelli, A., Trifoglio, M., Gianotti, F., Galli, M., Argan, A., Trois, A., Tavani, M., Moretti, E., Giuliani, A., Longo, F., Costa, E., Caraveo, P., Cattaneo, P. W., Chen, A., D'Ammando, F., De Paris, G., Di Cocco, G., Di Persio, G., Donnarumma, I., Evangelista, Y., Feroci, M., Ferrari, A., Fiorini, M., Lapshov, I., Lazzarotto, F., Lipari, P., Mereghetti, S., Morselli, A., Pacciani, L., Pellizzoni, A., Perotti, F., Picozza, P., Piano, G., Pilia, M., Prest, M., Pucella, G., Rapisarda, M., Rappoldi, A., Rubini, A., Sabatini, S., Soffitta, P., Striani, E., Vallazza, E., Vercellone, S., Vittorini, V., Zambra, A., Zanello, D., Antonelli, L. A., Colafrancesco, S., Cutini, S., Giommi, P., Lucarelli, F., Pittori, C., Santolamazza, P., Verrecchia, F., and Salotti, L. (2011). High spatial resolution correlation of AGILE TGFs and global lightning activity above the equatorial belt. *Geophys. Res. Let.*, 38:L14806.

Gallimberti, I., Bacchiega, G., Bondiou-Clergerie, A., and Lalande, P. (2002). Fundamental processes in long air gap discharges. *Comptes Rendus Physique*, 3(10):1335–1359.

GEANT Team (1993). GEANT - Detector description and simulation tool, CERN program library long write-up W5013. Technical report, CERN, Geneva.

Geant4 Collaboration (2018). Physics list guide. Available at https://geant4.web.cern.ch/node/1731#opt4.

Gjesteland, T., Østgaard, N., Laviola, S., Miglietta, M. M., Arnone, E., Marisaldi, M., Fuschino, F., Collier, A. B., Fabró, F., and Montanya, J. (2015). Observation of intrinsically bright terrestrial gamma ray flashes from the Mediterranean basin. *Journal of Geophysical Research (Atmospheres)*, 120:12.

Gjesteland, T., Østgaard, N., Nisi, R., Collier, A., Lu, G., Cummer, S., and Smith, D. (2014). Twelve Years of RHESSI TGFs - The second RHESSI TGF catalog. In *EGU General Assembly Conference Abstracts*, volume 16 of *EGU General Assembly Conference Abstracts*, page 14125.

Grefenstette, B., Smith, D., Hazelton, B., and Lopez, L. (2009). First RHESSI terrestrial gamma-ray flash catalog. *J. Geophys. Res.*, 114:A02314.

Gurevich, A., Milikh, G., and Roussel-Dupre, R. (1992a). Runaway electron mechanism of air breakdown and preconditioning during a thunderstorm. *Physics Letters A*, 165(5):463–468.

Gurevich, A. V., Milikh, G. M., and Roussel-Dupré, R. A. (1992b). Runaway electron mechanism of air breakdown and preconditioning during a thunderstorm. *Physics Letters A*, 165:463.

Hare, B. M., Uman, M. A., Dwyer, J. R., Jordan, D. M., Biggerstaff, M. I., Caicedo, J. A., Carvalho, F. L., Wilkes, R. A., Kotovsky, D. A., Gamerota, W. R., Pilkey, J. T., Ngin, T. K., Moore, R. C., Rassoul, H. K., Cummer, S. A., Grove, J. E., Nag, A., Betten, D. P., and Bozarth, A. (2016). Ground-level observation of a terrestrial gamma ray flash initiated by a triggered lightning. *Journal of Geophysical Research (Atmospheres)*, 121:6511–6533.

Hariharan, B., Chandra, A., Dugad, S. R., Gupta, S. K., Jagadeesan, P., Jain, A., Mohanty, P. K., Morris, S. D., Nayak, P. K., Rakshe, P. S., Ramesh, K., Rao, B. S., Reddy, L. V., Zuberi, M., Hayashi, Y., Kawakami, S., Ahmad, S., Kojima, H., Oshima, A., Shibata, S., Muraki, Y., and Tanaka, K. (2019). Measurement of the electrical properties of a thundercloud through muon imaging by the grapes-3 experiment. *Phys. Rev. Lett.*, 122:105101.

He, Y., Gu, B., Zhang, D., Lu, W.-Z., Yu, C. W., and Gu, Z. (2018). Towards the understanding of ice crystal-graupel collision charging in thunderstorm electrification.

Inan, U. S., Reising, S. C., Fishman, G. J., and Horack, J. M. (1996). On the association of terrestrial gamma-ray bursts with lightning and implications for sprites. *Geophys. Res. Let.*, 23(9):1017–1020.

Iudin, D. I., Sysoev, A. A., and Rakov, V. A. (2022). Problems of Lightning Initiation and Development. *Radiophysics and Quantum Electronics*, 64(11):780–803.

Janda, M., Machala, Z., Niklová, A., and Martišovitš, V. (2012). The streamer-to-spark transition in a transient spark: a dc-driven nanosecond-pulsed discharge in atmospheric air. *Plasma Sources Science and Technology*, 21(4):045006.

Klebesadel, R. W., Strong, I. B., and Olson, R. A. (1973). Observations of gamma-ray bursts of cosmic origin. *The Astrophysical Journal Letters*, 182:L85.

Krider, E. P. and Radda, G. J. (1975). Radiation field wave forms produced by lightning stepped leaders. 80(18):2653–2657.

Lin, Y. T., Uman, M. A., Tiller, J. A., Brantley, R. D., Beasley, W. H., Krider, E. P., and Weidman, C. D. (1979). Characterization of lightning return stroke electric and magnetic fields from simultaneous two-station measurements. *Journal of Geophysical Research: Oceans*, 84(C10):6307–6314.

Lindanger, A., Marisaldi, M., Maiorana, C., Sarria, D., Albrechtsen, K., Østgaard, N., Galli, M., Ursi, A., Labanti, C., Tavani, M., Pittori, C., and Verrecchia, F. (2020). The 3rd agile terrestrial gamma ray flash catalog. part i: Association to lightning sferics. *Journal of Geophysical Research: Atmospheres*, 125(11):e2019JD031985.

Lindanger, A., Marisaldi, M., Sarria, D., Østgaard, N., Lehtinen, N., Skeie, C. A., Mezentzev, A., Kochkin, P., Ullaland, K., Yang, S., Genov, G., Carlson, B. E., Köhn, C., Navarro-Gonzalez, J., Connell, P., Reglero, V., and Neubert, T. (2021). Spectral analysis of individual terrestrial gamma-ray flashes detected by asim. *Journal of Geophysical Research: Atmospheres*, 126(23):e2021JD035347. e2021JD035347 2021JD035347.

Lu, G., Blakeslee, R. J., Li, J., Smith, D. M., Shao, X.-M., McCaul, E. W., Buechler, D. E., Christian, H. J., Hall, J. M., and Cummer, S. A. (2010). Lightning mapping observation of a terrestrial gamma-ray flash. *Geophys. Res. Let.*, 37:L11806.

Lyu, F. and Cummer, S. A. (2018). Energetic radio emissions and possible terrestrial gamma-ray flashes associated with downward propagating negative leaders. *Geophysical Research Letters*, 45(19):10,764–10,771.

Lyu, F., Cummer, S. A., Briggs, M., Marisaldi, M., Blakeslee, R. J., Bruning, E., Wilson, J. G., Rison, W., Krehbiel, P., Lu, G., Cramer, E., Fitzpatrick, G., Mailyan, B., McBreen, S., Roberts, O. J., and Stanbro, M. (2016). Ground detection of terrestrial gamma ray flashes from distant radio signals. *Geophysical Research Letters*, 43(16):8728–8734.

Lyu, F., Cummer, S. A., Krehbiel, P. R., Rison, W., Bruning, E. C., and Rutledge, S. A. (2021). A distinct class of high peak-current lightning pulses over mountainous terrain in thunderstorms. *Geophysical Research Letters*, 48(14):e2021GL094153. e2021GL094153 2021GL094153.

Lyu, F., Cummer, S. A., and McTague, L. (2015). Insights into high peak current in-cloud lightning events during thunderstorms. *Geophysical Research Letters*, 42(16):6836–6843.

Mailyan, B. G., Briggs, M. S., Cramer, E. S., Fitzpatrick, G., Roberts, O. J., Stanbro, M., Connaughton, V., McBreen, S., Bhat, P. N., and Dwyer, J. R. (2016). The spectroscopy of individual terrestrial gamma-ray flashes: Constraining the source properties. *Journal of Geophysical Research (Space Physics)*, 121:11.

Marisaldi, M. (2020). Asim - fermi - agile simultaneous observation of terrestrial gamma-ray flashes. AGU Fall Meeting.

Marisaldi, M., Fuschino, F., Labanti, C., Galli, M., Longo, F., Del Monte, E., Barbiellini, G., Tavani, M., Giuliani, A., Moretti, E., Vercellone, S., Costa, E., Cutini, S., Donnarumma, I., Evangelista, Y., Feroci, M., Lapshov, I., Lazzarotto, F., Lipari, P., Mereghetti, S., Pacciani, L., Rapisarda, M., Soffitta, P., Trifoglio, M., Argan, A., Boffelli, F., Bulgarelli, A., Caraveo, P., Cattaneo, P. W., Chen, A., Cocco, V., D'Ammando, F., De Paris, G., Di Cocco, G., Di Persio, G., Ferrari, A., Fiorini, M., Froysland, T., Gianotti, F., Morselli, A., Pellizzoni, A., Perotti, F., Picozza, P., Piano, G., Pilia, M., Prest, M., Pucella, G., Rappoldi, A., Rubini, A., Sabatini, S., Striani, E., Trois, A., Vallazza, E., Vittorini, V., Zambra, A., Zanello, D., Antonelli, L. A., Colafrancesco, S., Gasparrini, D., Giommi, P., Pittori, C., Preger, B., Santolamazza, P., Verrecchia, F., and Salotti, L. (2010). Detection of terrestrial gamma ray flashes up to 40 MeV by the AGILE satellite. *Journal of Geophysical Research (Space Physics)*, 115:0.

Marisaldi, M., Fuschino, F., Tavani, M., Dietrich, S., Price, C., Galli, M., Pittori, C., Verrecchia, F., Mereghetti, S., Cattaneo, P. W., Colafrancesco, S., Argan, A., Labanti, C., Longo, F., Del

Monte, E., Barbiellini, G., Giuliani, A., Bulgarelli, A., Campana, R., Chen, A., Gianotti, F., Giommi, P., Lazzarotto, F., Morselli, A., Rapisarda, M., Rappoldi, A., Trifoglio, M., Trois, A., and Vercellone, S. (2014). Properties of terrestrial gamma ray flashes detected by AGILE MCAL below 30 MeV. *Journal of Geophysical Research (Space Physics)*, 119:1337–1355.

Marisaldi, M., Galli, M., Labanti, C., Østgaard, N., Sarria, D., Cummer, S. A., Lyu, F., Lindanger, A., Campana, R., Ursi, A., Tavani, M., Fuschino, F., Argan, A., Trois, A., Pittori, C., and Verrecchia, F. (2019). On the high-energy spectral component and fine time structure of terrestrial gamma ray flashes. *Journal of Geophysical Research: Atmospheres*, 124(14):7484–7497.

Marisaldi, M., Mezentsev, A., Sarria, D., Lindanger, A., Østgaard, N., Neubert, T., Reglero, V., Kochkin, P., Lehtinen, N., Maiorana, C., Skeie, C. A., Bjørge-Engeland, I., Ullaland, K., Genov, G., Christiansen, F., Christian, H., Al Nussirat, S., Briggs, M., Ursi, A., and Tavani, M. (2020). ASIM - Fermi - AGILE simultaneous observation of Terrestrial Gamma-ray Flashes. In *EGU General Assembly Conference Abstracts*, EGU General Assembly Conference Abstracts, page 12804.

Marshall, T. C. and Stolzenburg, M. (2001). Voltages inside and just above thunderstorms. *Journal of Geophysical Research: Atmospheres*, 106(D5):4757–4768.

McCarthy, M. and Parks, G. K. (1985). Further observations of x-rays inside thunderstorms. *Geophys. Res. Let.*, 12(6):393–396.

Millan, R. M., McCarthy, M. P., Sample, J. G., Smith, D. M., Thompson, L. D., McGaw, D. G., Woodger, L. A., Hewitt, J. G., Comess, M. D., Yand o, K. B., Liang, A. X., Anderson, B. A., Knezek, N. R., Rexroad, W. Z., Scheiman, J. M., Bowers, G. S., Halford, A. J., Collier, A. B., Clilverd, M. A., Lin, R. P., and Hudson, M. K. (2013). The Balloon Array for RBSP Relativistic Electron Losses (BARREL). *ssr*, 179(1-4):503–530.

Morgenstern, D., Stucke, I., Simon, T., Mayr, G. J., and Zeileis, A. (2022). Differentiating lightning in winter and summer with characteristics of the wind field and mass field. *Weather and Climate Dynamics*, 3(1):361–375.

Moss, G. D., Pasko, V. P., Liu, N., and Veronis, G. (2006). Monte carlo model for analysis of

thermal runaway electrons in streamer tips in transient luminous events and streamer zones of lightning leaders. *J. Geophys. Res.*, 111:A02307.

Østgaard, N., Albrecthsen, K. H., Gjesteland, T., and Collier, A. (2015). A new population of terrestrial gamma-ray flashes in the RHESSI data. *Geophys. Res. Let.*, 42:10.

Østgaard, N., Neubert, T., Reglero, V., Ullaland, K., Yang, S., Genov, G., Marisaldi, M., Mezentsev, A., Kochkin, P., Lehtinen, N., Sarria, D., Qureshi, B. H., Solberg, A., Maiorana, C., Albrechtsen, K., Budtz-Jørgensen, C., Kuvvetli, I., Christiansen, F., Chanrion, O., Heumesser, M., Navarro-Gonzalez, J., Connell, P., Eyles, C., Christian, H., and Al-nussirat, S. (2019). First 10 months of tgf observations by asim. *Journal of Geophysical Research: Atmospheres*.

Pallu, M., Celestin, S., Trompier, F., and Klerlein, M. (2021). Estimation of radiation doses delivered by terrestrial gamma ray flashes within leader-based production models. *Journal of Geophysical Research: Atmospheres*, 126(8):e2020JD033907. e2020JD033907 2020JD033907.

Pasko, V. P., Celestin, S., Bourdon, A., Janalizadeh, R., and Jansky, J. (2023). Conditions for inception of relativistic runaway discharges in air. *Geophysical Research Letters*, 50(7):e2022GL102710. e2022GL102710 2022GL102710.

Pu, Y., Cummer, S. A., Lyu, F., Briggs, M., Mailyan, B., Stanbro, M., and Roberts, O. (2019). Low frequency radio pulses produced by terrestrial gamma-ray flashes. *Geophysical Research Letters*, 46(12):6990–6997.

Rakov, V. A. and Kereszy, I. (2022). Ground-based observations of lightning-related x-ray/gamma-ray emissions in florida: Occurrence context and new insights. *Electric Power Systems Research*, 213:108736.

Rakov, V. A. and Uman, M. A. (2003). Electrical structure of lightning-producing clouds. In *Lightning*, pages 67–107.

Rison, W., Krehbiel, P. R., Stock, M. G., Edens, H. E., Shao, X.-M., Thomas, R. J., Stanley, M. A., and Zhang, Y. (2016). Observations of narrow bipolar events reveal how lightning is initiated in thunderstorms. *Nature Communications*, 7.

Rison, W., Thomas, R. J., Krehbiel, P. R., Hamlin, T., and Harlin, J. (1999). A gps-based three-dimensional lightning mapping system: Initial observations in central new mexico. *Geophys. Res. Let.*, 26:3573–3576.

Roberts, O. J., Fitzpatrick, G., Stanbro, M., McBreen, S., Briggs, M. S., Holzworth, R. H., Grove, J. E., Chekhtman, A., Cramer, E. S., and Mailyan, B. G. (2018). The First Fermi-GBM Terrestrial Gamma Ray Flash Catalog. *Journal of Geophysical Research (Space Physics)*, 123:4381–4401.

Roble, R. and Tzur, I. (1986). The global atmosphere electrical circuit. *The Earth's Electrical Environment*, pages 206–231.

Roussel-Dupré, R. and Gurevich, A. (1996). On runaway breakdown and upward propagating discharges. *J. Geophys. Res.*, 101(A2):2297–2311.

Régis, J.-M. (2011). *Fast Timing with LaBr 3 (Ce) Scintillators and the Mirror Symmetric Centroid Difference Method*. PhD thesis.

Saunders, C. (2008). Charge separation mechanisms in clouds. *Space Sci. Rev.*, 137:335–353.

Schonland, B. F. J. and Wilson, C. T. R. (1930). Thunder-storms and the penetrating radiation. *Proceedings of the Royal Society of London. Series A, Containing Papers of a Mathematical and Physical Character*, 130(812):37–63.

Shao, X.-M., Hamlin, T. D., and Smith, D. M. (2010). A closer examination of terrestrial gamma-ray flash-related lightning processes. *J. Geophys. Res.*, 115:A00E30.

Shao, X.-M., Ho, C., Caffrey, M., Graham, P., Haynes, B., Bowers, G., Blaine, W., Dingus, B., Smith, D., and Rassoul, H. (2018). Broadband rf interferometric mapping and polarization (bimap) observations of lightning discharges: Revealing new physics insights into breakdown processes. *Journal of Geophysical Research: Atmospheres*, 123(18):10,326–10,340.

Smith, D., Bowers, G., Kamogawa, M., Wang, D., Ushio, T., Ortberg, J., Dwyer, J., and Stock, M. (2018). Characterizing upward lightning with and without a terrestrial gamma ray flash. *Journal of Geophysical Research: Atmospheres*, 123.

Smith, D. M., Buzbee, P., Kelley, N. A., Infanger, A., Holzworth, R. H., and Dwyer, J. R. (2016). The rarity of terrestrial gamma-ray flashes: 2. RHESSI stacking analysis. *Journal of Geophysical Research (Atmospheres)*, 121:11.

Smith, D. M., Hazelton, B. J., Grefenstette, B. W., Dwyer, J. R., Holzworth, R. H., and Lay, E. H. (2010). Terrestrial gamma ray flashes correlated to storm phase and tropopause height. *Journal of Geophysical Research: Space Physics*, 115(A8).

Smith, D. M., Lopez, L. I., Lin, R. P., and Barrington-Leigh, C. P. (2005). Terrestrial gamma-ray flashes observed up to 20 mev. *Science*, 307(5712):1085–1088.

Stadnichuk, E., Svechnikova, E., Nozik, A., Zemlianskaya, D., Khamitov, T., Zelenyy, M., and Dolgonosov, M. (2021). Relativistic runaway electron avalanches within complex thunderstorm electric field structures. *Journal of Geophysical Research: Atmospheres*, 126(24):e2021JD035278. e2021JD035278 2021JD035278.

Stanley, M. A., Shao, X., Smith, D. M., Lopez, L., Pongratz, M., Harlin, J., Stock, M., and Regan, A. (2006a). A link between terrestrial gamma-ray flashes and intracloud lightning discharges. *Geophys. Res. Let.*, 33:L06803.

Stanley, M. A., Shao, X.-M., Smith, D. M., Lopez, L. I., Pongratz, M. B., Harlin, J. D., Stock, M., and Regan, A. (2006b). A link between terrestrial gamma-ray flashes and intracloud lightning discharges. *Geophysical Research Letters*, 33(6).

Stolzenburg, M. and Marshall, T. C. (2008). Charge structure and dynamics in thunderstorms. *Space science reviews*, 137(1-4):355–372.

Stolzenburg, M., Rust, W. D., and Marshall, T. C. (1998). Electrical structure in thunderstorm convective regions: 2. isolated storms. *Journal of Geophysical Research: Atmospheres*, 103(D12):14079–14096.

Stough, S. M. and Carey, L. D. (2020). Observations of anomalous charge structures in supercell thunderstorms in the southeastern united states. *Journal of Geophysical Research: Atmospheres*, 125(17):e2020JD033012. e2020JD033012 10.1029/2020JD033012.

Torii, T., Sugita, T., Kamogawa, M., Watanabe, Y., and Kusunoki, K. (2011). Migrating source of energetic radiation generated by thunderstorm activity. *Geophysical Research Letters*, 38(24).

Tran, M. D., Rakov, V. A., Mallick, S., Dwyer, J. R., Nag, A., and Heckman, S. J. (2015). A terrestrial gamma-ray flash recorded at the lightning observatory in gainesville, florida. *Journal of Atmospheric and Solar-Terrestrial Physics*, 136:86–93.

Tsuchiya, H., Enoto, T., Yamada, S., Yuasa, T., Nakazawa, K., Kitaguchi, T., Kawaharada, M., Kokubun, M., Kato, H., Okano, M., and Makishima, K. (2011). Long-duration $\gamma$ ray emissions from 2007 and 2008 winter thunderstorms. *Journal of Geophysical Research (Atmospheres)*, 116:D09113.

Uman, M. A., Swanberg, C. E., Tiller, J. A., Lin, Y. T., and Krider, E. P. (1976). Effects of 200 km propagation on florida lightning return stroke electric fields. *Radio Science*, 11(12):985–990.

US Department of Commerce, N. (2018). Lightning and planes.

Wada, Y., Enoto, T., Nakamura, Y., Furuta, Y., Yuasa, T., Nakazawa, K., Morimoto, T., Sato, M., Matsumoto, T., Yonetoku, D., Sawano, T., Sakai, H., Kamogawa, M., Ushio, T., Makishima, K., and Tsuchiya, H. (2019a). Gamma-ray glow preceding downward terrestrial gamma-ray flash. *Communications Physics*, 2(1):67.

Wada, Y., Enoto, T., Nakazawa, K., Furuta, Y., Yuasa, T., Nakamura, Y., Morimoto, T., Matsumoto, T., Makishima, K., and Tsuchiya, H. (2019b). Downward Terrestrial Gamma-Ray Flash Observed in a Winter Thunderstorm. *prl*, 123(6):061103.

Wada, Y., Morimoto, T., Nakamura, Y., Wu, T., Enoto, T., Nakazawa, K., Ushio, T., Yuasa, T., and Tsuchiya, H. (2022). Characteristics of low-frequency pulses associated with downward terrestrial gamma-ray flashes. *Geophysical Research Letters*, 49(5):e2021GL097348. e2021GL097348 2021GL097348.

Wang, D., Takagi, N., Gamerota, W. R., Uman, M. A., Hill, J. D., and Jordan, D. M. (2013). Initiation processes of return strokes in rocket-triggered lightning. *Journal of Geophysical Research: Atmospheres*, 118(17):9880–9888.

Wang, D., Wu, T., Huang, H., Yang, J., and Yamamoto, K. (2022). 3d mapping of winter lightning in japan with an array of discone antennas. *IEEJ Transactions on Electrical and Electronic Engineering*, 17(11):1606–1612.

Williams, E. R. (2010). Origin and context of c. t. r. wilson's ideas on electron runaway in thunderclouds. *Journal of Geophysical Research: Space Physics*, 115(A8).

Wilson, C. T. R. (1925). The electric field of a thundercloud and some of its effects. *Phys. Soc. London Proc.*, 32D:37.

Winn, W. P., Schwede, G. W., and Moore, C. B. (1974). Measurements of electric fields in thunderclouds. *Journal of Geophysical Research (1896-1977)*, 79(12):1761–1767.

Wu, T., Wang, D., Huang, H., and Takagi, N. (2021a). The strongest negative lightning strokes in winter thunderstorms in japan. *Geophysical Research Letters*, 48(21):e2021GL095525. e2021GL095525 2021GL095525.

Wu, T., Wang, D., and Takagi, N. (2021b). Compact lightning strokes in winter thunderstorms. *Journal of Geophysical Research: Atmospheres*, 126(15):e2021JD034932. e2021JD034932 2021JD034932.

Wu, T., Yoshida, S., Ushio, T., Kawasaki, Z., Takayanagi, Y., and Wang, D. (2014). Large bipolar lightning discharge events in winter thunderstorms in japan. *Journal of Geophysical Research: Atmospheres*, 119(2):555–566.

Xu, W., Celestin, S., and Pasko, V. P. (2014). Modeling of x-ray emissions produced by stepping lightning leaders. *Geophysical Research Letters*, 41(20):7406–7412.

Yoshida, S., Yoshikawa, E., Adachi, T., Kusunoki, K., Hayashi, S., and Inoue, H. (2019). Three-dimensional radio images of winter lightning in japan and characteristics of associated charge structure. *IEEJ Transactions on Electrical and Electronic Engineering*, 14(2):175–184.

Zhang, H., Lu, G., Lyu, F., Xiong, S., Ahmad, M. R., Yi, Q., Li, D., Xian, T., Yang, J., Liu, F., Zhu, B., Pu, Y., Cummer, S. A., Briggs, M. S., and Qie, X. (2021). On the terrestrial gamma-ray flashes preceding narrow bipolar events. *Geophysical Research Letters*, 48(8):e2020GL092160. e2020GL092160 2020GL092160.

Zhang, T., Yu, H., Zhou, F., Chen, J., and Zhang, M. (2018). Measurements of vertical electric field in a thunderstorm in a chinese inland plateau. *Annales Geophysicae*, 36(4):979–986.

Zhu, Y., Bitzer, P., Rakov, V., and Ding, Z. (2021). A machine-learning approach to classify cloud-to-ground and intracloud lightning. *Geophysical Research Letters*, 48(1):e2020GL091148.